

Deglacial and Holocene ~~Sea ice~~ and climate dynamics in the Bransfield Strait, at the Western-Northern Antarctic Peninsula

Maria-Elena Vorrath¹, Juliane Müller^{2,3,4}, Paola Cárdenas⁵, Thomas Opel², Sebastian Mieruch², Oliver Esper², Lester Lembke-Jene², Johan Etourneau^{6,7}, Andrea Vieth-Hillebrand⁸, Niko Lahajnar¹, Carina B. Lange^{5,9,10,11}, Amy Leventer¹², Dimitris Evangelinos^{7,13}, Carlota Escutia¹⁴, Gesine Mollenhauer^{2,3}

¹University Hamburg, Institute for Geology, Hamburg, Germany

²Alfred Wegener Institute, Helmholtz Centre for Polar and Marine Research, Bremerhaven, Germany

³MARUM – Center for Marine Environmental Sciences, University of Bremen, Germany

⁴Department of Geosciences, University of Bremen, Germany

⁵Centro de Investigación Dinámica de Ecosistemas Marinos de Altas Latitudes (IDEAL), Universidad Austral de Chile, Valdivia, Chile

⁶EPHE/PSL Research University, France

⁷UMR 5805 EPOC, CNRS, Université de Bordeaux, France

⁸Helmholtz Centre Potsdam GFZ German Research Centre for Geosciences, Potsdam, Germany

⁹Centro Oceanográfico ~~COPAS-CoastalSur-Austral~~ COPAS-Coastal, Universidad de Concepción, Chile

¹⁰Departamento de Oceanografía, Universidad de Concepción, Chile

¹¹Scripps Institution of Oceanography, La Jolla, CA 92037, USA

¹²Department of ~~Earth and Environmental Geosciences~~ Geology, Colgate University, New York, USA

¹³Departament de Dinàmica de la Terra i de l'Oceà, Universitat de Barcelona, Spain

¹⁴Instituto Andaluz de Ciencia de la tierra, CSIC-Univ. de Granada, Spain

Correspondence to: Juliane Müller, juliane.mueller@awi.de

Abstract

The reconstruction of past ~~sea-ice~~ sea-ice distribution in the Southern Ocean is crucial for an improved understanding of ice-ocean-atmosphere feedbacks and the evaluation of Earth system and Antarctic ice sheet models. The ~~Western~~-Antarctic Peninsula (WAP) is experiencing ~~rapid-a~~ rapid-a warming ~~since the start of regular monitoring of the atmospheric temperature in since the 1950ies.~~ since the start of regular monitoring of the atmospheric temperature in since the 1950ies. ~~Tand~~ the associated decrease in ~~sea-ice~~ sea-ice

30 cover contrasts the trend of growing ~~sea-ice~~ sea-ice extent in ~~eastern~~ East Antarctica. To reveal the long-term ~~sea~~
31 ~~ice~~ sea-ice history at the ~~Northern Antarctic Peninsula (NAP)~~ WAP under changing climate conditions we examined
32 a marine sediment core from the eastern basin of the Bransfield Strait covering the last Deglacial and the Holocene.
33 For ~~sea-ice~~ sea-ice reconstructions, we focused on the specific ~~sea-ice~~ sea-ice biomarker lipid IPSO₂₅, a highly
34 branched isoprenoid (HBI), and ~~sea-ice~~ sea-ice diatoms, whereas a phytoplankton-derived HBI triene (C_{25:3}) and
35 ~~warmer~~ open ocean diatom assemblages reflect predominantly ice-free conditions. We further reconstruct ocean
36 temperatures using glycerol dialkyl glycerol tetraether (GDGTs) and diatom assemblages, and compare our sea
37 ice and temperature records with published marine sediment and ice core data. ~~Our results document a retreat of~~
38 ~~the WAP ice shelf from at 13.89 ka BP on (before present). A m~~ Maximum sea-ice cover is observed during ~~at 12.9~~
39 ~~ka BP indicating the Antarctic Cold Reversal~~ 13,800-13,000 years before present (13.8 ka - 13 ka BP), while,
40 ~~seasonally ice-free conditions permitting (summer) phytoplankton productivity are reconstructed for the late~~
41 ~~Deglacial and the early Holocene from 13 ka to 8.3 ka BP. while a still extended but variable sea-ice coverage~~
42 ~~characterized the core site during the early Holocene from 11.7 ka to 8.2 ka BP. An overall decreasing sea-ice~~
43 ~~ice trend throughout the Middle Holocene is accompanied by coincides with a successive summer ocean warming~~
44 and increasing phytoplankton productivity. The Late Holocene is characterized by ~~a highly variable~~ unstable
45 ~~(winter) sea-ice~~ sea-ice ~~cover~~ concentration ~~conditions~~ and a ~~sustained decline in~~ further the duration and/or
46 ~~concentration of spring sea ice decline until 0.5 ka BP. Overall diverging trends in GDGT-based TEX86L and RI-~~
47 ~~OH' SOTs are found to be linked to opposing spring and summer insolation trends, respectively.~~

48
49 **Key Words:** ~~Bransfield Strait~~ Western Antarctic Peninsula, Holocene, ~~sea-ice~~ sea-ice cover, IPSO₂₅, highly
50 branched isoprenoids, diatoms, GDGTs

51 1 Introduction

52 Sea ice significantly affects the global climate system through its impact on the atmosphere-ocean exchange of
53 heat and gas, ~~the~~ physical and chemical properties of the water masses, ocean circulation, primary production and
54 biogeochemical cycles (Chisholm, 2000; Vancoppenolle et al., 2013). ~~Sea-ice~~ Sea-ice cover limits evaporation,
55 affects precipitation and increases the reflection of solar radiation due to a high albedo (Allison et al., 1982;
56 Butterworth and Miller, 2016; Turner et al., 2017). When sea ice forms, cold and dense brines develop,
57 contributing to the formation of intermediate and deep waters (Nicholls et al., 2009). Importantly, ~~the down-~~
58 ~~welling of~~ these dense water masses ~~can~~ prevent warm currents from reaching the continental ~~slope-shelf where~~
59 ~~they stimulate the basal melt and stimulating basal melt~~ of Antarctic ice shelves, with implications for the stability

60 of ice sheets and ~~eventually~~ global sea level (Cook et al., 2016; Escutia et al., 2019; Etourneau et al., 2019; Hellmer
61 et al., 2012; Huss and Farinotti, 2014). During the spring season, ~~sea ice~~ melting ~~stimulates~~ boosts marine
62 primary production by seeding algal cells, ~~the release of~~ releasing nutrients and by promoting ocean stratification
63 and a shallow mixed layer depth (Arrigo et al., 1997; Vernet et al., 2008). In addition, nutrient supply can be
64 locally enhanced by ~~increasing~~ wind-driven upwelling activity along the ~~sea ice~~ edge, ~~thus triggering~~
65 ~~phytoplankton blooms~~ (Alexander and Niebauer, 1981). Enhanced carbon fixation through this ~~nutrient~~ ice-
66 stimulated biological pump hence leads to an increase of biological material transport and organic carbon export
67 to the ocean floor, thus ~~contributing to lower~~ lowering surface $p\text{CO}_2$ (Han et al., 2019; Kim et al., 2004; Schofield
68 et al., 2018; Wefer et al., 1988).

69 Since satellite-based sea-ice data became available in 1979, fast and profound changes have been observed ~~both~~
70 ~~in the Arctic and as well as West Antarctica~~ ~~globally due and ascribed~~ to anthropogenic global warming (IPCC,
71 2021). The Western Antarctic Peninsula (WAP), in particular, is experiencing a rapid warming of the atmosphere
72 (Carrasco et al., 2021; Vaughan et al., 2003) and the ocean (Cook et al., 2016). This ~~is~~ accompanied
73 ~~by~~ rapidly retreating glaciers and ice shelves (Cook et al., 2016; Rignot et al., 2019) and by
74 ~~significant~~ ~~remarkable~~ ~~remarkably~~ loss of ~~sea ice~~ cover in the adjacent seas (Parkinson and Cavalieri, 2012).

75 For an assessment of the region's past sensitivity to climate change, the deglacial and Holocene climate history of
76 the Antarctic Peninsula (AP) has been studied extensively. The Deglacial, the transition from the Last Glacial
77 Maximum (LGM, Clark et al., 2012) to the Holocene, is characterized by a rapid warming punctuated by a distinct
78 cold event, the so-called Antarctic Cold Reversal (ACR) from 14.7 ka to 13 ka BP (EPICA Community Members,
79 2004; Mulvaney et al., 2012; Pedro et al., 2016). This drastic cooling of both atmosphere and ocean temperatures
80 ~~in the high~~ ~~southern latitudes~~ is well reflected in ~~recorded by~~ stable isotope records of ~~in~~ Antarctic ice cores and
81 ~~within~~ marine sediments (Blunier and Brook, 2001; Domack et al., 2001; Jouzel et al., 1995; Morigi et al., 2003;
82 Stenni et al., 2001). From the Deglacial towards the Middle Holocene, the Antarctic Peninsula Ice Sheet (APIS)
83 retreated rapidly from the outer shelf to its modern configuration with ~~heavy~~ high melt water discharge (Bentley
84 et al., 2014). Several ~~syntheses~~ ~~comparisons between~~ marine and lacustrine of Holocene climate records ~~reflected~~
85 ~~in~~ ~~reflected from~~ marine and lake sediment cores reveal that the timing of both hydrological and environmental
86 changes ~~was~~ is highly variable ~~across~~ at the WAP (Allen et al., 2010; Ingólfsson et al., 2003; Minzoni et al., 2015;
87 Roseby et al., 2022; Sjunneskog and Taylor, 2002; Totten et al., 2022). ~~The ice core records from James Ross~~
88 ~~Island (JRI) at the northeastern tip of the AP shows a pronounced warming between about 12 and 11 ka BP~~
89 ~~followed by a cooling trend until about 9 ka BP and stable temperatures until 2.5 ka BP. From 2.5 ka BP in the~~
90 ~~Late Holocene cooling was reversed since temperatures cooled until 0.6 ka BP (Mulvaney et al., 2012).~~ An overall

91 consensus, ~~however~~, is that WAP ocean temperatures were in the WAP was, in comparison to the Deglacial or the
92 Late Holocene, warmer during the Early and Middle Holocene ~~Optimum~~, i.e. between 12 ka and 4 ka BP
93 (Shevenell et al., 2011). In contrast, marine sediment records show many multiple different climate patterns for the
94 Late Holocene ~~shows many different climate patterns~~ around the AP, including a continuous Neoglacial cooling
95 (Etourneau et al., 2013), ~~whereas other records other studies resolve warmer and colder phases such as the~~
96 Medieval Climate Anomaly and/or the Little Ice Age (Bentley et al., 2009).
97 Knowledge of past Southern Ocean sea-ice sea-ice variability is crucial ~~to for~~ accurately modelling climate
98 feedbacks ~~impacting the Antarctic ice sheet stability since the LGM~~ (Crosta et al., 2022). For periods beyond the
99 satellite era, information on past sea-ice conditions knowledge is based on proxies from marine sediments, ~~and~~ ice
100 cores (e.g. Bracegirdle et al., 2015, 2019; Crosta et al., 2022; Escutia et al., 2019; Thomas et al., 2019), and snow
101 petrel stomach oil deposits (McClymont et al., 2022). At present, most climate mModels, however, do not
102 only often fail to reproduce seasonal sea-ice cycles observed sea-ice sea-ice trends of the satellite era; simulated sea
103 ice sea-ice conditions reconstructions and observations of sea-ice for both glacial and interglacial periods and also
104 often disagree with geological proxies (Green et al., 2022; Lhardy et al., 2021; Roche et al., 2012). Ice-core based
105 sea-ice sea-ice reconstructions for the LGM are primarily use based on the concentrations of sea salt sodium (WAIS
106 Divide Project Members, 2015). However, since sea salt aerosols might be overprinted by the highly variable
107 wind direction and meteorological conditions in Antarctica, and thus not reflect sea salt records may not sufficiently
108 be consistent in reflecting regional sea-ice sea-ice conditions (Thomas et al., 2019). Although marine sediment
109 records usually mostly have a lower temporal resolution than ice cores, they marine proxy reconstructions can
110 resolve regional and depending on the spatial distribution of sediment cores - of/ or large-scale changes in sea
111 ice sea-ice conditions, as well as sea surface and subsurface ocean temperature, primary productivity and marine
112 ecology (Hillaire-Marcel and de Vernal, 2007). In addition to commonly used geochemical, lithological and
113 microfossil proxies (e.g. ice rafted debris (IRD), diatom assemblages, total organic carbon), new approaches focus
114 on specific organic biomarkers - highly branched isoprenoids (HBIs) - as reliable proxies to distinguish between
115 open marine and seasonally sea ice covered environments. The di-unsaturated HBI IPSO₂₅ (Ice Proxy for the
116 Southern Ocean, C_{25:2}, Belt et al., 2016; Massé et al., 2011) that is produced by sea-ice algae and deposited on the
117 ocean floor after the sea-ice melt in spring has already been applied ~~for in~~ Antarctic sea-ice sea-ice reconstructions
118 (e.g. Barbara et al., 2013; Denis et al., 2010; Etourneau et al., 2013). Following the phytoplankton-PIP₂₅- sea-ice
119 index (-PIP₂₅) approach for the Arctic (Müller et al., 2011), IPSO₂₅ has been combined with phytoplankton-
120 derived- HBI trienes and/or sterols phytoplankton to determine the phytoplankton-IPSO₂₅ sea-ice index called
121 PIPSO₂₅ (Vorrath et al., 2019), which has been successfully evaluated with recent Antarctic spring sea-ice

concentrations (Lamping et al., 2021). Other studies applied PIPSO₂₅ and examined its potential for sea-ice sea-ice reconstructions over periods of the industrial era (Vorrath et al., 2020) and over deglacial and Holocene time intervals in has been used in paleo sea ice studies from the Amundsen Sea (Lamping et al., 2020). Hence, the combination to Combining these new molecular proxies with the classical diatom assemblage approach and/or geochemical ice core proxies provides offers a thorough assessment of unique opportunity to robustly reconstruct past sea-ice sea-ice conditions at the WAP.

Here, we present a marine sediment record covering the past 13.89 ka BP and to reconstruct Deglacial and Holocene environmental conditions in the eastern northern Bransfield Strait at the NAP at the northernmost position of the WAP. Our study is based on a multiproxy approach focusing on the sea-ice sea-ice biomarker IPSO₂₅, an open ocean marine phytoplankton biomarker (HBI triene), and on glycerol dialkyl glycerol tetraether lipids (GDGTs) for subsurface ocean temperatures (SOT). Additional estimates information of primary productivity, about the probability of winter sea-ice sea-ice coverage (WSI) and summer sea surface temperature (SSST) comes from bulk sediment organic carbon and biogenic silica contents and diatom assemblages using transfer functions, respectively. In an intercomparison, we evaluate the different approaches to reconstruct sea-ice sea-ice conditions and ocean temperatures. and We discuss. We compare discuss and compare our proxy results in regard of with other marine sediment and ice core records spanning the Holocene providing further insight into the environmental dynamics at the Antarctic Peninsula across the Deglacial and the Holocene.

2 Material and Methods

2.1 Study Area

The Bransfield Strait is located between the NWAP and the South Shetland Islands (SSI) (Fig. 1a), comprising a trough (> 2000 m) lying between a narrow shelf to the north (SSI) and a broad shelf area to the south (AP). Within this area, a shallow shelf and deeper depressions characterize the Bransfield Basin with water depths exceeding 2000 m (Fig. 1b). The shelf areas were affected by intense ice sheet dynamics during the last glaciation (Canals and Amblas, 2016b; Ingólfsson et al., 2003) leaving ice sheet grounding lines and glacial troughs on the sea-floor (Canals et al., 2016; Canals and Amblas, 2016a).

The modern Bransfield Basin is influenced by complex oceanic current systems, which are not fully constrained because three different water masses enter the basin from the east and west (Moffat and Meredith, 2018; Sangrà et al., 2011) and their mixing is not well understood. The cold (< 0 °C) and relatively salty Weddell Sea Water (WSW) enters from the east, flows alongshore the peninsula and fills the Bransfield Strait basins below 150 m water depth surface. The WSW is also observed at greater depths (200–600 m) north of the SSI (outer shelf) and

152 at Elephant Island due to wind-driven modulation (Meijers et al., 2016). In the western part of the Bransfield Strait,
153 the WSW mixes with warmer a second water mass, the Bellingshausen Sea Water (BSW; 0 - 50 m water depth)
154 and Circumpolar Deep Water (CDR; 200 - 550 m water depth; Collares et al., 2018; Sangrà et al., 2011, 2017),
155 which ~~are~~ transported in a branch of the Antarctic Circumpolar Current (ACC) over the Anvers Shelf. It conveys
156 well-stratified, fresh and warmer (> 0 °C) surface water to a depth of about 50 m (Sangrà et al., 2011). A third
157 water mass ~~Also originating from the ACC is a third, deeper water mass. Originating from the Circumpolar Deep~~
158 Water (CDW), that is present between 200 m and 550 m (Sangrà et al., 2017). BSW and CDW flow eastward
159 along the SSI, turn around and flow westward at the northern tip of the islands (Sangrà et al., 2011). BSW and
160 WSW forms the subsurface Bransfield front with the CDW at depth and the surface Peninsula Front (PF) with the
161 WSW, that runs parallel to the Antarctic mainland (Sangrà et al., 2011, 2017). The interplay of currents leads to a
162 stratification of the water column of pronounced pycnocline within the upper 20 m of the water column in summer,
163 with accompanied by a steep temperature gradient in the first-upper 100 m, as below sea surface. This can be
164 observed in CTD-hydrographic profiles from the Bransfield Basin that show a dominance of WSW below 200
165 m (see Fig. 1c and Sangrà et al., 2011). The eddy system at the Peninsula Front is assumed to play a key role for
166 mixing and upwelling of the different surface and subsurface water masses (Sangrà et al., 2011; Zhou et al., 2002),
167 while several glaciers from the WAP influence coastal surface water due to meltwater discharge and also transport
168 dense bottom waters to the Bransfield Basin (Meredith et al., 2018).
169 Modern sea ice sea-ice conditions at the core site in the eastern Bransfield Strait are characterized by a mean winter
170 sea ice sea-ice concentration of ca. 50%, which declines to 18% and less than 2% sea ice sea-ice concentration
171 during spring and summer, respectively (cf. Vorrath et al., 2019). ~~Modern sea ice conditions follow a declining~~
172 trend in all seasons with a nearly sea ice free summers (Hobbs et al., 2016; Vorrath et al., 2020). ~~While atmospheric~~
173 temperatures show a rising trend since the 1950ies ocean temperatures (Carrasco et al., 2021), ocean temperatures
174 are increasingly influenced by warm water intrusions and higher sea surface temperatures (Martinson and McKee,
175 2012; Meredith and King, 2005). At the core site, mean annual sea surface temperatures are -0.6 °C with up to 0.8
176 °C during summer (WOA 18; Boyer et al., 2018; Locarnini et al., 2018).
177 Primary production in the Bransfield Strait is mainly driven by mixing of water masses at the fronts (Gonçalves-
178 Araujo et al., 2015), mixed layer depth and upwelling (Sangrà et al., 2011), sea ice sea-ice dynamics (Vernet et al.,
179 2008) and iron availability (Klunder et al., 2014). High concentrations of chlorophyll *a* and diatoms are distributed
180 north of the Peninsula Front PF and at the SSI, while lower production and communities of nanoplanktonic
181 plankton nanoflagellates are found between the Peninsula Front and the WAP (Gonçalves-Araujo et al., 2015).
182 Further, changes in coastal primary production are driven by upwelling, elevated iron distribution availability, as

Formatiert: Schriftart: Kursiv

183 well as the nutrient release and surface water stratification generated by melting sea ice in the austral spring and
184 the retreat of sea ice cover in spring releasing nutrients and stabilizing the water column (Vernet et al., 2008). A
185 close-robust link between marine primary production at the surface in surface waters and the sediment composition
186 at the underlying ocean floor is reflected in high concentrations of total organic carbon (TOC), pigments, sterols
187 and diatoms (Cárdenas et al., 2019), and supported by studies confirming high fluxes of sinking particles (Kim et
188 al., 2004; Wefer et al., 1988). In the study area, particle flux is highly variable with seasonal peaks occurring in
189 late spring, which accounts for 85% of the total flux (Ducklow et al., 2008). Lithologically, the sediments consist
190 mainly of ~~terrestrial-terri~~genous silt and clay with varying amounts of diatom mud and ooze, and sand (Cádiz
191 Hernández, 2019; Lamy, 2016; Wu et al., 2019).

193 2.2 Sediment samples and age model

194 Piston core PS97/072-1 (62° 0.39' S, 56° 3.86' W, 1993 m water depth, 1583 cm in length) was recovered in the
195 eastern Bransfield Strait Basin during R/V *Polarstern* cruise PS97 (Lamy, 2016) (Fig. 1). The ~~sediment~~ core is
196 dominated by silt with thin layers of sand, clay, and traces of volcanic ash. Single pebbles are present below 630
197 cm. ~~The core is disturbed~~ Since we found disturbed sediments below 1015 cm depth and we only considered
198 samples from above this level for our analyses. ~~After an XRF scan the core sampling for different analytical~~
199 ~~approaches~~ was done at the Alfred Wegener Institute (AWI) where ~~the the-~~ samples were stored frozen in glass
200 vials (for biomarker analysis) and at 4 °C in plastic bags (for micropaleontology).

201 The age model of core PS97/072-1 is based on ¹⁴C-radiocarbon dating of eight ~~ealeite-benthic foraminiferal and~~
202 ~~mollusk fragments~~ samples with the mini carbon dating system (MICADAS) available at AWI (Mollenhauer et
203 al., 2021). From the conventional ¹⁴C age we subtracted a reservoir age based on modelling by Butzin et al. (2017)
204 and also subtracted an estimated ventilation age of 1200 years ~~that we derived from ages between paired planktic~~
205 ~~and benthic foraminifera of 1000 to 1500 years found off Chile (Siani et al., 2013) and Kerguelen Islands~~
206 ~~(Gottschalk et al., 2020) to account for the considerable water depth of our site (see table supplement section 1).~~
207 ~~before~~ After the subtraction we calibrated the ages with the calibration curve SHIntCal20 (Reimer et al., 2020)
208 (Hogg et al., 2020) to calendar years before present (cal BP) with Calib 7.1 (Stuiver et al., 2018). To estimate the
209 ~~top~~ age of the core top, TOC and biogenic opal data of the piston core were matched with data from a multicore
210 from the same sampling site that has been previously dated via ²¹⁰Pb (Vorrath et al., 2020; supplement section 2).
211 Ages of sediments below the oldest radiocarbon date (868.5 cm; 12.04 ka BP) were ~~extrai~~nterpolated assuming a
212 constant sedimentation rate. ~~The downcore ages between the lowest radiocarbon dates sample and the core~~
213 ~~bottom was interpolated based on previous sedimentation rates.~~ We applied the Bayesian age modelling tool

Formatiert: Deutsch (Deutschland)

Formatiert: Deutsch (Deutschland)

Feldfunktion geändert

Feldfunktion geändert

Formatiert: Deutsch (Deutschland)

Formatiert: Deutsch (Deutschland)

Formatiert: Deutsch (Deutschland)

Formatiert: Deutsch (Deutschland)

Feldfunktion geändert

214 *hummingage*, a freely available tool developed at AWI, that has been successfully applied in previous studies (e.g.
215 Ronge et al., 2021). ~~As the lack of age constraints between 12 ka and 6 ka BP may introduce chronological~~
216 ~~uncertainties, we only focus on overall trends reflected in our data and refrain from detailed allocations of known~~
217 ~~climatic events in this older time period.~~

218 **2.3 Organic geochemical analyses of piston core PS97/072-1**

219 For the analyses of ~~the bulk~~ several organic ~~geochemical composition~~ components and biomarkers, ~~the~~ 334
220 ~~sediments~~ ~~samples~~ were freeze-dried and homogenized in an agate mortar. ~~Prior to sediment homogenization,~~
221 ~~coarse grains were separated using a sieve (500 µm mesh size).~~ Total carbon (C) and nitrogen (N) were measured
222 with a CNS analyzer (Elementar Vario EL III, error of standards and duplicates < 5%). ~~Total organic carbon (TOC)~~
223 was measured on 0.1 g of acidified samples (500 µl HCl) and determined in a carbon-sulphur determinator (CS-
224 800, ELTRA, standard error < 0.6%). To identify the source of TOC, measurements of stable carbon isotopes of
225 bulk organic matter were done at Universität Hamburg (UHH), Germany, and at Washington State University
226 (WSU), USA. At UHH, the samples were acidified three times with 100 µl 1 N HCl and dried on a hotplate. High-
227 temperature combustion was done in an Elementar CHNOS Vario isotope elemental analyser at 950 °C and the
228 analysis was conducted with an Elementar IsoPrime 100 isotope ratio mass spectrometer. We calibrated the pure
229 tank CO₂ with the International Atomic Energy Agency reference standards IAEA-CH6 and IAEA-CH7. These
230 and two other standards (IVA Sediment and Sucrose) acted as internal standards in the measurement. The error of
231 continuous standard duplicates was < 0.2‰ and < 0.06‰ for sample duplicates. At WSU, 100 mg of freeze-dried
232 sediment samples were used. An elemental analyzer coupled with an Isoprime isotope ratio mass spectrometer
233 (IRMS) was used, with a precision of 0.1‰. The running standard was a protein hydrolysate calibrated against
234 NIST standards. Isotope ratios are expressed in units per mil (‰). δ¹³C values are expressed in ‰ against Vienna
235 Pee Dee Belemnite (VPDB).

236 Biogenic opal was estimated ~~on 327 samples~~ following the alkaline extraction procedure described by Mortlock
237 and Froelich (1989), but using 0.5M NaOH as a digestion solution (Müller and Schneider, 1993). Extraction and
238 analysis by molybdate-blue spectrophotometry were conducted at the University of Concepción, Chile. Values are
239 expressed as biogenic opal by multiplying the Si (%) by 2.4 (Mortlock and Froelich, 1989). ~~Opal values could be~~
240 ~~somewhat overestimated by 2 - 2.5% since we~~ We did not correct for the release of extractable Si from coexisting
241 clay minerals, ~~and thus biogenic opal values could be slightly overestimated~~ (Schlüter and Rickert, 1998).
242 Instrumental precision was ±0.5%; error of duplicates ≤ 3%. Details on the methodology used can be found in
243 Cárdenas et al. (2019).

244 The extraction, purification and identification of 137 samples to identify HBIs followed the analytical protocol
245 published e.g. in Belt et al. (2014) and Vorrath et al. (2019). Prior to extraction, 40 µl 7-hexylnonadecane (7-HND;
246 0.0019 µg/µl) and 100 µl C₄₆(0.0098 µg/µl) were added served as internal standards. Lipids were extracted using
247 ultra sonication and a mixture of CH₂Cl₂:MeOH (v/v 2:1; 6 ml). HBIs and GDGTs were separated by means of
248 open column chromatography using SiO₂ as the stationary phase and hexane, and CH₂Cl₂:MeOH (v/v 1:1) as
249 eluents. HBIs were analyzed by means of an Agilent 7890B gas chromatograph (30 m DB 1MS column, 0.25 mm
250 diameter, 0.250 µm film thickness) coupled to an Agilent 5977B mass spectrometer (MSD, 70 eV constant
251 ionization potential, ion source temperature 230 °C). The initial oven temperature of 60 °C was held for 3 min,
252 ramped to 325 °C within 23 min, and was held at 325 °C for 16 min. HBIs were identified *via* comparison of
253 their retention times (IPSO₂₅ and HBI triene with RI 2084DB-1MS and 2046DB-1MS, respectively) and mass
254 spectra with published mass spectra (Belt, 2018) and quantified using the ratio of peak areas of individual HBIs
255 (*m/z* 346; *m/z* 348) and the 7-HND (*m/z* 266)- standard and consideration of instrumental response factors. The
256 error of duplicates was <1.4% for IPSO₂₅, <2.6% for HBI trienes. The phytoplankton-IPSO₂₅ index (PIPSO₂₅) was
257 calculated after Vorrath et al. (2019) as:

$$258 \text{PIPSO}_{25} = \frac{\text{IPSO}_{25}}{\text{IPSO}_{25} + (c \times \text{phytoplankton marker})} \quad (1)$$

259 The concentrations of the phytoplankton-derived HBI/HBI z-triene are was is considered as a phytoplankton
260 biomarker and, since the concentrations in these samples are were on at the same level as IPSO₂₅, and the c-factor
261 was hence set to 1 (Vorrath et al., 2019). To confirm the sea-ice origin of IPSO₂₅, the stable carbon isotope
262 composition of IPSO₂₅ was examined in 8 samples (with minimum 50 ng carbon) via GC-irm-MS at the GFZ
263 Potsdam, Germany. The GC (7890N Agilent) equipped with an Ultra1 column (50 m x 0.2 mm diameter, 0.33 µm
264 film thickness) was connected to a DeltaVPlus isotope ratio mass spectrometer through a modified GC-Isolink
265 interface. Each sample was separated chromatographically using with a temperature program that started with an
266 oven temperature of 80 °C, which was held for 3 min, ramped to 250 °C with 3 °C per min and then ramped to
267 320 °C with 5 °C per min and finally reached temperature of 325 °C with a ramp of 1 °C per min and held for
268 15 min. The organic substances of the GC effluent stream were oxidized to CO₂ in the combustion furnace held at
269 940 °C on a CuO/Ni/Pt catalyst. Samples were measured in duplicate and the standard deviation was ≤0.5 %. The
270 quality of the isotope measurements was checked regularly (for each analysis) by measuring different *n*-alkane
271 standards with known isotopic composition of n-C15, n-C20, n-C25 (in equal concentration) and n-C16 to n-C30
272 (in various concentrations)—~~provided~~ by Campro Scientific, Germany and Arndt Schimmelmann, Indiana
273 University, USA).

Formatiert: Nicht Hochgestellt/ Tiefgestellt

274 GDGTs were re-dissolved in 120 μ l hexane:isopropanol (v/v 99:1) and filtered through polytetrafluoroethylene
 275 filters (0.45 μ m in diameter) and analyzed using high performance liquid chromatography (HPLC, Agilent 1200
 276 series HPLC system) coupled to a single quadrupole mass spectrometer (MS, Agilent 6120 MSD) via an
 277 atmospheric pressure chemical ionization (APCI) interface. The individual GDGTs were separated at 30 °C on a
 278 Prevail Cyano column (150 mm x 2.1 mm, 3 μ m). After injection of the sample (20 μ l) it passed a 5 min isocratic
 279 elution with mobile phase A (hexane/2-propanol/chloroform; 98:1:1, flow rate 0.2 ml/min). The mobile phase B
 280 (hexane/2-propanol/chloroform; 89:10:1) was increased to 100% in two steps: a linear increase to 10% over 20
 281 min followed by an increase to 100% within 10 min. During the measurement, the column was cleaned after 7 min
 282 via backflush (5 min, flow 0.6 ml/min) and re-equilibrated with solvent A (10 min, flow 0.2 ml/min). The
 283 conditions of the APCI were a nebulizer pressure of 50 psi, vaporizer temperature and N₂ drying gas temperature
 284 350 °C, flow 5 l/min, capillary voltage 4 kV, and corona current 5 μ A. Following Liu et al. (2020), iGDGTs and
 285 branched GDGTs were detected by selective ion monitoring (SIM) of (M+H⁺) ions (dwell time 76 ms) using
 286 their molecular ions (GDGTs-I (m/z 1300), GDGTs-2 (m/z 1298), GDGTs-3 (m/z 1296), crenarchaeol (m/z 1292)
 287 and GDGTs-Ia (m/z 1022), GDGTs-IIa (m/z 1036), GDGTs-IIIa (m/z 1050)) and quantified. In relation to the
 288 internal standard C₄₆ (m/z 744), the molecular ions m/z of GDGTs I (m/z 1300), GDGTs II (m/z 1298), GDGTs
 289 III (m/z 1296), and crenarchaeol (m/z 1292) were quantified. Also, the branched GDGTs Ia (m/z 1022), GDGTs
 290 IIa (m/z 1036), GDGTs IIIa (m/z 1050) were quantified. The hydroxylated GDGTs OH-GDGT-0 (m/z 1318), OH-
 291 GDGT-1 (m/z 1316), and OH-GDGT-2 (m/z 1314) were quantified in the scans of their related GDGTs (Fietz et
 292 al., 2013). The standard deviation was 0.01 units of TEX₈₆^L.

293 Kalanetra et al. (2009) showed that GDGT-producing Thaumarchaeota are abundant in subsurface marine waters
 294 in both Arctic and Antarctic regions. As Thaumarchaeota were found between 50 m and 200 m water depth in
 295 Antarctica (Kim et al., 2012), temperatures based on GDGTs are suggested to reflect sub-surface waters
 296 (Etourneau et al., 2013, 2019). Similarly, also RI-OH' based temperatures in Prydz Bay have been interpreted to
 297 reflect subsurface water temperatures (Liu et al., 2020). We therefore consider our results to reflect subsurface
 298 ocean temperatures (SOTs). We calculated TEX₈₆^L after Kim et al. (2012) with the m/z 1296 (GDGT-3), m/z
 299 1298 (GDGT-2), m/z 1300 (GDGT-1):

$$300 \quad \text{TEX}_{86}^L = \log \left(\frac{[\text{GDGT-2}]}{[\text{GDGT-1}] + [\text{GDGT-2}] + [\text{GDGT-3}]} \right)$$

301 (2)

302 and calibrated with SOT = 50.8 * TEX₈₆^L + 36.1 (Kim et al., 2012). (3)

303 For the calculation of temperatures based on hydroxylated GDGTs we followed the approach of Lü et al. (2015)

304
$$RI - OH' = \frac{[OH-GDGT-1]+2 \times [OH-GDGT-2]}{[OH-GDGT-0]+[OH-GDGT-1]+[OH-GDGT-2]} \quad (4)$$

305 and calibrated it with SOT = (RI-OH' - 0.1) / 0.0382. (5)

306 For the branched and isoprenoid tetraether (BIT) index for indicating terrestrial organic matter (Hopmans et al.,
307 2004) we used crenarchaeol (m/z 1292) and the branched GDGTs and calculated it as:

308
$$BIT = \frac{[GDGT-1a]+[GDGT-11a]+[GDGT-111a]}{[Crenarchaeol]+[GDGT-1a]+[GDGT-11a]+[GDGT-111a]} \quad (6)$$

309

310 **2.4 Diatom analyses**

311 We selected a set of 76 samples for the analysis of diatom assemblages. At first, sampling resolution was every
312 40-50 cm; thereafter, and based on the biogenic opal results, resolution was increased (every 8 cm) at intervals
313 with high variability. ~~and then was increased~~ Freeze-dried samples (20-120 mg) were treated with hydrogen
314 peroxide and sodium pyrophosphate to remove organic matter and clays, respectively, washed several times with
315 DI water until reaching neutral pH. The treated samples were then settled for six hours in B-Ker2 settling chambers
316 to promote an even distribution of settled particles (Scherer, 1994; Schrader and Gersonde, 1978; Warnock and
317 Scherer, 2015). Once the samples were dry, the quantitative slides were mounted with Norland mounting medium
318 (refraction index=1.56). Diatom valves per slide were counted across traverses (at least 400 valves per slide) using
319 an Axioscop 2 Plus and Olympus BX60 at a magnification of ×1000. The counting procedure and definition of
320 counting units followed those of Schrader and Gersonde (1978). We performed two sets of counts, with and
321 without *Chaetoceros* resting spores. Diatoms were identified to species or species group level and, if applicable,
322 to variety or form level following the taxonomy described by e.g., Gersonde and Zielinski (2000), Armand and
323 Zielinski (2001), Esper et al. (2010), Esper and Gersonde (2014a, 2014b). Diatom ~~studies-analyses~~ were done by
324 the same investigator at the University of Concepción, Chile, and at Colgate University, USA.

325 Because diatom distribution in the Southern Ocean is directly associated with the temperature zonation and the
326 frontal systems of the ACC (Cárdenas et al., 2019; Esper et al., 2010; Esper and Gersonde, 2014a, 2014b; Zielinski
327 and Gersonde, 1997), diatom species were grouped into ecological assemblages reflecting i) seasonal sea ice –
328 associated with temperatures -1.8 to 0°C; ii) cold open ocean – associated with the maximum sea-ice extent in
329 winter and temperatures between 1 and 4°C; iii) warmer open ocean – with temperatures between 4 and 14°C, and
330 iv) benthic-epiphytic habitats (Buffen et al., 2007; Cárdenas et al., 2019). Additionally, a group of reworked
331 diatoms was identified (supplement section 6). Diatom species were grouped into ecological assemblages reflecting
332 i) seasonal sea_ice, ii) cold open ocean, iii) warmer open ocean, and iv) benthic-epiphytic diatoms environments
333 (Buffen et al., 2007; Cárdenas et al., 2019; Esper et al., 2010) (specific group composition is described in detail in

Formatiert: Englisch (Vereinigtes Königreich)

Formatiert: Englisch (Vereinigtes Königreich)

334 ~~supplement section 3). Additionally, a group of reworked diatoms was identified.~~ A Spearman principal
335 component analysis (PCA) was applied to the diatom assemblages to differentiate their temporal distribution.
336 For estimation of winter ~~sea ice~~ (WSI) concentrations, we applied the transfer function MAT-D274/28/4an
337 ~~to the total diatom counts (including Chaetoceros resting spores). The transfer function which~~ comprises 274
338 reference samples with 28 diatom taxa/taxa groups and considers an average of 4 analogues (Esper and Gersonde,
339 2014a). ~~Further, the transfer function retrieved the 4 lowest squared chord distances as a measure for assemblage~~
340 ~~similarity for each sample depth, which does not automatically equal the 4 closest geographical reference samples.~~
341 ~~However, analysis of the geographical location of the retrieved analogues identified 4 major source regions for the~~
342 ~~sediment core, with 38.9% of all reference samples coming from the seasonal sea-ice zone of the Scotia Sea, 33.2%~~
343 ~~from the summer sea-ice zone of the coastal Amundsen Embayment, 18.4% from the summer sea-ice zone of the~~
344 ~~coastal Weddell Sea, and 8.9% from the summer sea-ice zone of the Ross Sea. Thus, about 72% of all retrieved~~
345 ~~samples represent Atlantic Ocean environment, and about 60% of all retrieved samples represent a polar coastal~~
346 ~~environment similar to the region of the analyzed core. The analogues refer to surface sediments from the Atlantic,~~
347 ~~Pacific and western Indian sector of the Southern Ocean. There are 10 analogues from the immediate vicinity of~~
348 ~~the Antarctic Peninsula.~~ The WSI renders sea ice concentrations in a 1° by 1° grid for the September average of
349 the period 1981 to 2010 (Reynolds et al., 2002, 2007). The threshold ~~of an~~ between the open ocean ~~and the~~ sea
350 ~~ice~~ covered area is set at 15% of ~~sea ice~~ concentration (Zwally et al., 2002) and the average ~~sea~~
351 ~~ice~~ edge is defined at 40% (Gersonde et al., 2005; Gloersen et al., 1993). ~~The qualitative estimation of sea~~
352 ~~ice concentration was derived from the abundance pattern of diatom sea-ice indicators (Gersonde and Zielinski,~~
353 ~~2000).~~ The estimation of summer sea surface temperature (SSST) came from the transfer function IKM-
354 D336/29/3q comprising 336 reference samples (Pacific, Atlantic and Indian Southern Ocean) with 29 diatom taxa
355 and three factors (Esper and Gersonde, 2014b). The calculations ~~for WSI~~ were done with the software R (R Core
356 Team, 2012) using the packages Vegan (Oksanen et al., 2012) and Analogue (Simpson and Oksanen, 2012).

357 3 Results

358 Based on our age model, ~~the~~ sediment core PS97/072-1 covers the last 13.89 ka BP with a mean sedimentation
359 rate of 67 cm/ka and a temporal resolution ranging between 50 and 150 years per sample interval. We note a higher
360 sedimentation rate of 95 cm/ka between 5.5 ka and 3 ka BP and few short-term intervals of significantly
361 particularly lowered (19 cm/ka) and higher enhanced (190 cm/ka) sedimentation (Fig. 2).

362 Organic geochemical bulk parameters (TOC, biogenic opal), concentrations of HBIs (IPSO₂₅, C_{25:3} HBI triene) and
363 diatom species of warmer open ocean conditions and sea ice assemblages of piston core PS97/072-1 are

364 summarized in Figure 3 (additional data can be found in the supplement section 34). TOC increases from very low
365 values of 0.1 wt% at 13.7 ka BP to an average concentration of ~0.8 wt% between 9.9 ka BP and the top of the
366 core with recurring short-lived minima down to 0.03 wt% during the Middle and Late Holocene (Fig. 3f). Some
367 of these TOC minima ~~may be associated with~~ occur within thin sandy layers of volcanic ash. Biogenic opal shows
368 a similar pattern with minimum values in the lower part of the record (3.2 wt% at 13.0 ka BP) and increases
369 throughout the Deglacial to Holocene with average values of 30 wt% and a maximum of 54.4 wt% at 5.3 ka BP
370 (Fig. 3e).

371 Between 13.89 ka and 13.4 ka BP, both IPSO₂₅ and HBI triene concentrations are close to or below the detection
372 limit (0.1 µg g⁻¹ TOC). ~~Throughout the record, the~~ The IPSO₂₅ concentration ranges between 0.1 to 31.5 µg g⁻¹
373 TOC, while the concentration of the HBI triene ranges between 0.1 and 6.6 µg g⁻¹ TOC (Fig. 3). IPSO₂₅ is absent
374 before 13.5 ka BP and rises rapidly to maximum values of 31.5 µg g⁻¹ TOC at 12.89 ka BP. Subsequently,
375 concentrations decrease steadily until 8.5 ka BP and then remain at a stable n-average level of ~4 µg g⁻¹ TOC
376 with a slightly decreasing trend to 1 µg g⁻¹ TOC towards between 3.0 ka BP the present and smaller peaks of 10
377 µg g⁻¹ TOC at 6.0 and 3.0 ka BP. ~~Only traces of the HBI triene occur at very low concentrations is largely absent~~
378 until 13.0 ka BP, while its concentration -and- increases to shows high elevated concentrations up to 6.6 µg g⁻¹ TOC
379 after 8.5 ka BP with large fluctuations of more than 5 µg g⁻¹ TOC in the Middle Holocene and from 3.4 ka BP to
380 the present.

381 The diatom composition has two contrasting groups indicating open ocean conditions, a cold water assemblage
382 and a warmer water assemblage, and a seasonal sea ice assemblage (Fig. 3; see supplement section 3). The diatom
383 composition has two contrasting groups indicating warm open ocean conditions (Fig. 3a) and seasonal sea ice (Fig.
384 3e). Although the group reflecting seasonal sea ice is also present throughout the core (mostly >20%), the highest
385 contributions are seen before 13.3 ka BP and -between 10.8 and 9.9 ka BP and around 3 ka BP. The contribution
386 of the warmer open ocean assemblage is very low in the Deglacial and Early Holocene, and rises to highest values
387 in the Middle Holocene and remains around 10% in the Late Holocene. A biplot of a principal component analysis
388 (PCA) shows the relationship of the ecological groups along the sediment core for three time intervals with clear
389 dominance of seasonal sea ice before 13.3 ka BP and warmer open ocean conditions after 8.5 ka BP (supplement
390 section 5 and 64).

391 Winter Sea ice sea-ice concentration estimates based on diatom assemblages (WSI) and the PIPSO₂₅ index as well
392 as the content of IRD in PS97/072-1 are summarized in figure 4 (a-c). Reconstructed winter sea ice sea-ice
393 concentrations (% WSI) derived from the MAT transfer function results from the diatom assemblages range from
394 80% to 90% during the ACR and the Deglacial (13.89 ka – 11 ka BP) and exhibit an overall decreasing trend over

395 the Middle Holocene with distinct fluctuations reaching minimum sea-ice concentrations of ca. 65% during
396 the Middle and Late Holocene (Fig. 4a). PIPSO₂₅ values show a similar trend indicating higher sea-ice cover
397 during the ACR, the Deglacial and the Early Holocene (PIPSO₂₅ > 0.8) and a successive decline to 0.5 on average
398 throughout the Middle and Late Holocene with a distinct minimum at 0.5 ka BP (Fig. 4b). IRD (lithic particles
399 and pebbles > 500 µm) occurs frequently between 13.89 ka and 9 ka BP and is virtually absent in the younger part
400 of the sediment core (Fig. 4c).

401 Figure 5 provides ocean temperature anomalies reconstructions based on diatom assemblages (SSST) and GDGT-
402 derived RI-OH⁺ and TEX₈₆^L SOTs in core PS97/072-1 (Fig. 5 b-d). Diatom-derived SSST estimates derived from
403 diatom data generally depict lower minimum temperatures of -1.5 °C to 0 °C during the Deglacial and Early
404 Holocene, accompanied by and a shift to ca. 1 °C warming temperatures trend (to > 0 °C) in the Middle and
405 Late Holocene with a distinct cold event at 3.1 ka BP (Fig. 5b). A short cold event with a SSST decrease of ca. 1.5
406 °C occurred around 3.1 ka BP. Similar to SSSTs, also RI-OH⁺-derived SOTs likewise reflect generally lower
407 temperatures during the Deglacial and Early Holocene, and between -1.9 to -1.2 °C and a similar trend of rising
408 0.4 °C warmer temperatures in the Middle and Late Holocene to -1.2 °C until 4.2 ka BP followed by a subtle
409 cooling to -1.4 °C (Fig. 5c). TEX₈₆^L-derived SOTs data from GDGTs cover a temperature range of 0.7 to 3.8 °C
410 and display an opposite trend to both SSST and RI-OH⁺ SOT with peak temperatures decreasing temperatures to
411 0.7 °C since from during the Deglacial and an overall Holocene cooling towards present (Fig. 5d).

412

413 4 Discussion

414 4.1 The late Deglacial (13.814 ka to 11.7 ka BP)

415 In the oldest part of our sediment record, covering the later part of the last Deglacial from 13.814 ka until 11.7 ka
416 BP, we observe a remarkable environmental change indicated by significant large shifts in the TOC, biomarker
417 and diatom records (Fig. 3). Before 13.4 ka BP, the very low concentrations of HBI biomarkers (Fig. 3b and d),
418 TOC (Fig. 3f), and biogenic opal (Fig. 3e) between 13.8 ka and 13.5 ka BP suggest that primary production of
419 phytoplankton associated with open marine conditions and also sea-ice algae synthesizing IPSO₂₅ settings
420 was diminished low, while sea-ice related diatom species show the highest contribution of 73% (Fig. 3c), albeit
421 with very low concentrations (supplement section see online resource 5). Highest WSI concentrations values of
422 winter sea ice Highest (WSI, Fig. 4a) and PIPSO₂₅ values spring sea ice (PIPSO₂₅, Fig. 4a, b) indicators and WSI
423 values are pointing towards a maximum heavy sea-ice cover that lasted until summer in both seasons and
424 are. Lowest and lowest ocean temperatures reflected in the RI-OH⁺-derived SOTs are well in line with peak ssNa

Formatiert: Tiefgestellt

425 concentrations and minimum $\delta^{18}\text{O}$ values in the EDML and WAIS and JRI ice core records, referring to an
426 extended ~~sea ice~~ cover until 13 ka BP and lowered atmospheric temperatures (Fig. 4; EPICA Community
427 Members, 2006; Fischer et al., 2007; WAIS Divide Project Members, 2015). We note that for the interpretation of
428 PIPSO₂₅ values, changes in both IPSO₂₅ and HBI triene concentrations need to be evaluated carefully to reliably
429 deduce information on ~~sea ice~~ conditions. High PIPSO₂₅ values may refer to an extended ~~sea ice~~
430 cover that lasts until summer (thus hampering phytoplankton productivity/HBI triene synthesis), whereas low
431 PIPSO₂₅ values point to a reduced ~~sea ice~~ cover in terms of duration (in spring) and/or ~~sea ice~~
432 concentration. ~~In agreement with the biogenic opal and~~ The near absence of IPSO₂₅, the HBI triene and ~~and~~
433 warm open ocean diatom species as well as minimum contents in TOC and biogenic opal between 13.89 ka and
434 13.5 ka BP evidences a ~~very thick or~~ permanent, potentially perennial sea ice cover or at least sea ice that was
435 ~~too thick to allow photosynthesis of sea ice algae inhabiting at the sea ice bottom~~. Similarly, Lamping et al.
436 (2020) related the absence of IPSO₂₅ and a ~~phytoplankton-derived dinosterol~~ biomarker in sediments in the
437 western Amundsen Sea to the re-advance of a floating ice shelf canopy during the ACR. At the PS97/072-1 core
438 site in the eastern Bransfield Strait, both the presence of perennial sea ice, or an ice shelf tongue extending from
439 the APIS, could explain the lack of indicators of phytoplankton productivity and IPSO₂₅-synthesizing ice algae.
440 We hence assume that the very low absolute concentrations of sea ice-associated diatoms result from lateral
441 transport underneath the ice or reworking of sediments older than 13.5 ka BP. ~~The~~ abrupt increase in IPSO₂₅
442 concentrations at 13.5 ka BP, ~~however,~~ may indicate the retreat or thinning of such an ice-shelf cover/canopy, from
443 the core site permitting ~~sea ice~~ algae growth during spring and a subsequent increase in primary production
444 reflected in rapidly rising HBI triene concentrations since 13 ka BP (Fig. 3b, d). Such a transition from a perennial
445 floating ice canopy to conditions characterized by (seasonal) ~~sea ice~~ cover is also reported by Milliken et
446 al. (2009) for the nearby Maxwell Bay (King George Island; SSI) between 14 ka and 10 ka BP. Interestingly, ~~A~~
447 ~~significant prominent~~ decrease in sea ice associated diatoms between 13 ka and 12 ka BP (Fig. 3c), ~~however,~~ is
448 not mirrored by the still high WSI concentrations. This discrepancy could relate to a weaker preservation potential
449 of certain diatoms reflecting seasonal sea ice (e.g. *Synedropsis* sp., *Nitzschia stellata*) that are not considered within
450 the transfer function to estimate WSI, which highlights the need to examine silica dissolution effects for the
451 interpretation of diatom records. We note that traces of biomarkers and diatoms (supplement section 4 and 65)
452 deposited in sediments older than 13.5 ka BP may reflect sub-ice shelf lateral advection and reworking (Smith et
453 al., 2019).
454 With regard to the ocean temperatures recorded at core site PS97/072-1, we note that the overall cool deglacial
455 temperatures derived from diatom data (SSST) and hydroxylated GDGTs (RI-OH') seem to be linked to the

Formatiert: Tiefgestellt

Formatiert: Tiefgestellt

Formatiert: Tiefgestellt

Formatiert: Tiefgestellt

456 lowered summer insolation (Fig. 5a), whereas higher TEX_{86}^L temperatures seem to be associated with a higher low
457 spring insolation (Fig. 5d). ~~While~~ The impact of seasonality on GDGT-based ocean temperature estimates is still
458 under debate and would require further improvements in ~~on~~ regional calibrations. ~~The~~ The observation of maximum
459 abundances of thaumarchaeota species (producing isoGDGTs applied to determine TEX_{86}^L) in Antarctic coastal
460 waters during spring (Kalanetra et al., 2009; Murray et al., 1998), however, seems to support our interpretation
461 and also helps to explain the divergent trends in TEX_{86}^L and RI-OH' derived SOT estimates, as the latter proxy
462 might be also sourced by other archaea species that probably grow mostly during the summer season.

463 While the ACR lasts from 14.7 ka to 13 ka BP (Pedro et al., 2016) as indicated by e.g. the WAIS Divide ice core
464 records from JRI (Fig. 5h, Mulvaney et al., 2012) and WAIS Divide (Fig. 5i, WAIS Divide Project Members,
465 2013), our sediment record shows that cold conditions with an extended sea-ice cover, limiting summer
466 phytoplankton productivity (Fig. 4a, b) and reduced summer ocean temperatures in the eastern Bransfield Strait,
467 lasted until ca. 11 ka BP (Figs. 4 and 5). Further, the Deglacial and Early Holocene (Fig. 4e) IRD content (Fig.
468 4c; including the presence of single large pebbles) in core PS97/072-1 points to the frequent occurrence of
469 icebergs during the Deglacial and the Early Holocene (Fig. 4e), which relates related to ~~related to~~ evidencing the overall ice
470 sheet disintegration along the WAP that occurred around 14 ka BP at the SSI South Shetland Islands and promoted
471 seasonally open-marine conditions at Anvers-Hugo Trough at 13.6 ka BP (middle WAP shelf) and at 123.92
472 ka BP in at Palmer Deep at the southern (inner WAP shelf), respectively AP (Domack et al., 2001; Domack, 2002;
473 Jones et al., 2022; Milliken et al., 2009; Roseby et al., 2022). At our core site, rising RI-OH' SOTs and a slight
474 decrease in PIPSO₂₅ values and rising RI-OH' SOTs characterize the late Deglacial between 13 ka and 11.7 ka BP
475 (Fig. 4b, 5c). A prominent decline in large-scale sea-ice cover is also reflected in the decreasing ssNA
476 concentrations in the EDML and WAIS ice cores between 13 ka and 11.7 ka BP (Fig. 4e, f) and is likely related
477 to a distinct atmospheric warming, as reflected in ice core stable water isotopes (Fig. 5h).

478 The ACR cooling and the subsequent Late Deglacial This subsurface ocean warming ~~This subsurface ocean~~ warming may relate to inter-
479 hemispheric teleconnections through a global reorganization of atmospheric and ocean circulation that is
480 associated with ~~related to~~ the bipolar seesaw pattern of opposite climate trends between the northern and southern
481 hemisphere (Anderson et al., 2009; Broecker, 1998; EPICA Community Members, 2006; Pedro et al., 2016; Stenni
482 et al., 2011). While a northward shift of the southern westerlies during the ACR (Fletcher et al., 2021) promoted
483 Antarctic sea-ice expansion and glacier readvance (potentially affecting causing an ice cover over the
484 PS97/072-1 core site), a ~~With~~ cooling of the northern hemisphere and with a southward shift of the
485 Intertropical Convergence Zone and the southern hemisphere westerlies (Lamy et al., 2007) resulted in intensified
486 wind stress in the Drake Passage (Timmermann et al., 2007). and This pattern would have increased upwelling

487 that may have driven the continued ocean warming and sea-ice retreat in Antarctica towards the Holocene
488 (Anderson et al., 2009).

489

490 **4.2 Early Holocene warming from 11.7 ka to 8.2 ka BP**

491 The Early Holocene from 11.7 ka to 8.2 ka BP is characterized by a progressively decreasing spring sea-ice cover
492 inferred from shown by declining PIPSO₂₅ values (Fig. 4b), as well as though highly variable winter and spring
493 sea-ice cover with prominent as shown by further declining WSI shifts in sea-ice concentration (from
494 90% to 65%: and PIPSO₂₅ values (Fig. 4a and b). These WSI fluctuations are not reflected in the sea ice diatom
495 assemblage, which, similar to the biogenic opal content, follows an increasing trend until 10.5 ka BP (Fig. 3c, e).
496 Increased Improved accumulation of biogenic opal and a better preservation of (thin-walled) sea-ice-related
497 diatoms that are not used for the transfer function may explain the mismatch between the WSI record and sea ice
498 diatom assemblage. The increase in While biogenic opal is further accompanied by a rising and TOC contents
499 exhibit increasing trends, while concentrations of the HBI triene and warm open ocean diatoms remain low and,
500 only an significant increase after 9 ka BP, signal signalling suggests higher phytoplankton productivity (Fig. 3a,
501 b). Diatom-derived SSSTs exhibit marked fluctuations but remain relatively low until 8.2 ka BP (Fig. 5b). RI-OH⁺
502 and TEX₃₆^L SOTs display diverging trends following the summer and spring insolation, respectively (Fig. 5).
503 Ocean temperatures based on warming is indicated by RI-OH⁺ based SOT, while TEX₃₆^L SOT and diatom-derived
504 SSST show fluctuating temperatures without a clear trend (Fig. 5b, c and d).

505 While PIPSO₂₅ values display a rather gradual decrease in sea-ice coverage, the WSI record suggests a
506 highly variable sea-ice cover, with several few distinct sea ice minima between 11 ka and 10 ka BP and
507 around 9 ka BP (Fig. 4a and b). These sea ice minima may have resulted from punctuated warming events, e.g.
508 around 10 ka BP, when SSST shows a short temperature peak, which might have led to a delayed sea-ice
509 formation in autumn and winter (Fig. 5b). Another WSI minimum at 9 ka BP coincides with a major, final (and
510 final) peak in IRD deposition at the core site (Fig. 4), evidencing iceberg discharge during episodes of peak AP
511 ice-sheet loss retreat and enhanced calving at the WAP (Jones et al., 2022). As sea-ice melting may have
512 been an important driver of the ocean stratification, we suggest warmer, stratified surface waters with moderate
513 production in summer, supported by increasing summer insolation in December (Fig. 5a). Ameliorating climate
514 conditions, ice-shelf retreat along the NAP and the establishment of modern-like ocean conditions after 9 ka BP
515 have also been proposed for the western Bransfield Strait by (Heroy et al. (2008) and are well in line with the
516 rising concentrations contribution of warm open ocean diatoms and the phytoplankton-derived HBI triene at our
517 core site after 9 ka BP (Fig. 3). The general decrease in spring sea-ice cover (reflected in declining PIPSO₂₅

Formatiert: Schriftart: Kursiv

518 values) Our marine records of decreasing sea ice may have been fostered by and high a maximum spring and rising
519 summer insolation (Fig. 5a, d), and subsurface ocean temperatures shortening the duration of sea ice sea-ice cover.
520 Rising RI-OH' temperatures are which are consistent with the overall slight warming trend recorded in the WAIS
521 Divide ice core (Fig. 5h), which has been shown to be mainly driven by increasing summer temperatures (Jones
522 et al., 2022). Interestingly, neither this rise in RI-OH' derived SOTs nor the highly variable The decreasing
523 TEX₈₆^L SOT temperature trends at core site PS97/072-1 corresponds to the declining TEX₈₆ temperatures reported
524 for ODP site 1098 in at Palmer Deep (Fig. 5g; Shevenell et al., 2011) though the latter displays a more pronounced
525 temperature drop (of ca. 6 °C) between 11.7 ka and 8.2 ka BP, or the declining δD values recorded in the JRI ice
526 core (Fig. 5; Mulvaney et al., 2012). These regional differences may relate to changing ocean circulation patterns,
527 and associated shifts in water mass distribution along the WAP and EAP, and the local post-glacial environmental
528 development during the Early Holocene. Deposition of laminated diatom oozes in the Anvers-Hugo Trough at the
529 WAP middle shelf during the early Holocene since 11.5 ka BP, for example, g., documents episodes of extremely
530 high productivity in response to a southward shift of the southern hemisphere westerlies and the advection of warm
531 and nutrient-rich CDW (Roseby et al., 2022). We propose that the eastern Bransfield Strait remained mainly
532 "inaccessible" for CDW and BSW until further ice recession between 10 ka and 5 ka BP (Ó Cofaigh et al., 2014
533 and references therein) permitted advection of these water masses into the Bransfield Strait. We further note that
534 the partly opposing trends in RI-OH' and TEX₈₆^L temperatures at our core site could indicate that the respective
535 GDGT-producing archaea thrive in different water depths or during different seasons.

536

537 **4.3 Middle Holocene from 8.2 ka until 4.2 ka BP**

538 The Middle Holocene from 8.2 ka to 4.2 ka BP was a period of significant remarkable sea ice sea-ice retreat and
539 minimum iceberg flux activity records at the core site indicated by decreasing WSI and PIPSO₂₅ values and
540 virtually absent IRD (Fig. 4), and an oceanic warming reflected in SSST and RI-OH' SOT (Fig. 4 and 5). For
541 the whole period, diatoms associated with warmer open ocean conditions, peak HBI triene concentrations and
542 maximum TOC and as well as biogenic opal contents (Fig. 3) indicate refer to a high export production during the
543 Middle Holocene (Abelmann et al., 2006; Smetacek et al., 2004). These higher primary productivity export
544 productivity production is can be linked to a decrease in of both winter and spring sea ice and potentially ice-free
545 summers indicated by WSI and PIPSO₂₅ minima, respectively (Fig. 4a, b), and elevated SSSTs and (summer)
546 SOTs (Fig. 5b, c) promoting ice-free summer ocean conditions favorable for phytoplankton productivity. These
547 Middle Holocene sea-ice conditions compare well with the modern situation at the core site characterized by a

Formatiert: Schriftart: Kursiv

548 seasonal decrease in ~~sea ice~~ sea-ice concentration from 50% during winter to mainly ice-free summers (NSIDC;
549 Cavalieri et al., 1996). ~~like it was observed for modern sea ice conditions in this region (Vorrath et al., 2020).~~
550 The ~~continued~~ retreat of the previously grounded ~~APISAP ice sheet adjacent to over the Bransfield Strait~~ between
551 10 ka and 5 ka BP finally opened the passage for ACC ~~surface~~ waters to enter the Bransfield Strait from the west
552 (Bentley et al., 2014; Ó Cofaigh et al., 2014). As a result, we suggest that ~~sea ice~~ sea-ice conditions at our core site
553 were ~~predominantly~~ influenced by ~~branches incursions of warmer oceanic waters carried associated with~~ the
554 ACC (~~i.e. the BSW and CDW~~) ~~leading to a shorter sea ice season and/or less intensive sea ice cover, while and cold~~
555 ~~water inflow and sea ice~~ advection from the Weddell Sea was diminished due to the still grounded ice sheet
556 at the tip of the AP (Ó Cofaigh et al., 2014), ~~leading to a shorter sea ice~~ sea-ice season in the eastern Bransfield
557 Strait. This shift towards a warmer, less ice-covered ocean setting in ~~the~~ eastern Bransfield Strait is ~~well in line~~
558 ~~with~~ reflected in the transition from proximal to distal glacial marine conditions in Maxwell Bay (Milliken et al.,
559 2009) and may be associated with the Mid-Holocene climatic optimum. This timing contrasts the ~~notion~~ of Heroy
560 et al. (2008), who, ~~based on diatom assemblage analyses of a sediment core in the western Bransfield Strait,~~
561 ~~confined~~ the Mid-Holocene climatic optimum to a shorter time interval between 6.8 ka and 5.9 ka BP ~~based on~~
562 ~~diatom assemblage analyses of a sediment core in the western Bransfield Strait.~~ We propose that this temporal
563 offset may relate to regionally different responses, ~~to~~ glacial retreat patterns impacting oceanic pathways and the
564 position of frontal systems controlling primary productivity within ~~the~~ Bransfield Strait. The generally decreasing
565 WSI and variable PIPSO₂₅ values further depict different trends than PIPSO₂₅ values determined for the JPC10 in
566 Palmer Deep (Fig. 4d; Etourneau et al., 2013), which suggest an overall increase in spring sea ice along the WAP
567 until 4.2 ka BP. Though minima in spring sea ice at 7.5 ka, 6.5 ka and 5.4 ka BP at core site PS97/072-1 may ~~be~~
568 ~~related compare~~ to PIPSO₂₅ minima observed for JPC10, the lack of Middle Holocene age ~~constraint~~ tie points in
569 our core from the Bransfield Strait ~~deters~~ prevents us from concluding on a common driver ~~causing~~ for these ~~sea~~
570 ~~ice~~ sea-ice reductions. ~~minima in spring sea ice at 6.5 ka and 5.4 ka BP~~ The weak influence from the Weddell Sea
571 ~~limited the export of cold waters and supported~~ was weak and opposite sea ice conditions were reconstructed for
572 ~~in the eastern AP where HBI biomarker and diatom assemblages record~~ regionally extended sea ice cover between
573 7 ka and 4.5 ka BP (Fig. 4e, Barbara et al., 2016a; Minzoni et al., 2015).

574 Regarding ocean temperatures, we observe a sustained warming in RI-OH' SOT₂, punctuated by a cooling at 5.5
575 ka BP (Fig. 5c), while TEX₈₆¹ temperatures depict a subtle cooling of ~~ca. 0.5 to 0.9~~ °C between 8.2 ka and 7 ka
576 BP, followed by a warm reversal ~~of up to 3.1~~ °C until 6 ka BP, and a further cooling until 4.2 ka BP (Fig. 5e).
577 This Middle Holocene slight cooling trend is ~~also has also been~~ observed in the TEX₈₆¹ records ~~at~~ from the core
578 ~~sites core sites at in~~ Palmer Deep at the WAP (Fig. 4 and 5f, g; Etourneau et al., 2013; Shevenell et al., 2011).

579 The similarity between these records encourages us to assume that these TEX₈₆-derived temperatures from along
580 the WAP and NAP are driven by spring insolation rather than ~~reflecting~~being a reflection of annual mean ocean
581 temperature conditions (~~see above~~), and contrasts a rapid warming observed in JPC38 from the eastern AP
582 between 8 ka and 6.5 ka BP (Fig. 1 and 5, Barbara et al., 2016; Etourneau et al., 2019). Here, the near coastal
583 marine sediment core close to JRI (Fig. 5g, Barbara et al., 2016) records the transition from cold and heavily sea
584 ice covered conditions at 8.2 ka BP to a warmer water environment with reduced sea ice cover permitting more
585 phytoplankton growth between 6.5 ka and 4.2 ka BP (Barbara et al., 2016). Since stable temperatures are inferred
586 from the JRI ice core during the entire Middle Holocene (Mulvaney et al., 2012), we suggest that the environmental
587 changes recorded in JPC38 reflect ocean-driven rather than atmospheric processes.

589 **4.4 Late Holocene and Neoglacial from 4.2 ka BP until today**

590 The Late Holocene covering the past 4.2 ka BP is characterized by a highly variable winter sea ice and decreasing
591 spring ~~sea ice~~sea-ice cover at core site PS97/072-1, as indicated ~~reflected~~in the MAT-derived WSI and a decline
592 in PIPSO₂₅ values over the past 2 ka (Fig. 4a, b). Rather constant ~~relatively stable environmental conditions at our~~
593 ~~core site reflected in constant biogenic opal and TOC contents (Fig. 3e, f), however, suggest that primary~~
594 ~~productivity remained relatively unaffected by this reduction in spring sea ice cover.~~ While decreasing
595 IPSO₂₅ concentrations between 2.5 ka BP and the core top (Fig. 3d) suggest a reduced productivity of the sea ice
596 diatom species synthesizing this molecule, no significant changes are observed in the sea ice diatom assemblage
597 (Fig. 3c), which supports the assumption that only a restricted group of diatoms - at least *Berkeleya adeliensis* -
598 produce IPSO₂₅ (Belt et al., 2016). The warm open ocean diatom assemblage follows an overall declining trend
599 throughout the Late Holocene, which is not reflected in the highly variable and slightly increasing HBI triene
600 concentrations (Fig. 3a, b), and a prominent decrease in HBI triene concentrations occurs only at 1 ka BP, ~~which~~
601 ~~display a slight increase until it decline and still variable but elevated HBI triene concentrations. A gradual decline~~
602 ~~in PIPSO₂₅ values between 4.2 ka and 1.5 ka BP contrasts the highly variable WSI concentrations (Fig. 4). ... While~~
603 ~~the observation of cooler sea surface temperatures, and a diminished spring sea ice cover indicated by the~~
604 ~~joint decrease in the warm open ocean diatom assemblage and PIPSO₂₅ values since 2 ka BP may seem~~
605 ~~counterintuitive, Milliken et al. (2009) report a similar development in Maxwell Bay since 2.6 ka BP. Interestingly,~~
606 ~~records of diatom and radiolarian assemblages of a sediment core (Gebra-2) collected in very close vicinity to~~
607 ~~PS97/072-1 document an overall increase in sea-ice taxa over the past 3 ka BP with distinct Neoglacial events~~
608 ~~characterized by higher (denser and longer) sea ice cover (Bárcena et al., 1998). The lower sampling~~
609 ~~resolution and missing age control for the past 3 ka BP in PS97/072-1, however, hamper a more detailed~~

Formatiert: Schriftart: Kursiv

610 comparison of diatom species in our core with those investigated for Gebra-2. The Neoglacial increase in (spring)
611 sea ice cover is also indicated by a prominent rise of PIPSO₂₅ values determined for JPC10 in Palmer Deep
612 (Fig. 4d; Etourneau et al., 2013). Similarly, deposition of ssNa in the EDML ice core (Fischer et al., 2007)
613 increases since 2 ka BP.

614 Minimum PS97/072-1 PIPSO₂₅ values at 0.5 ka BP result from a ~~reduced~~ ~~to the significantly-notably~~ reduced
615 IPSO₂₅ and HBI triene concentrations (Fig. 3b, d). While similar to our observation for the Deglacial, this pattern
616 of ~~minimum~~ low HBI triene and ~~minimum-lowest~~ IPSO₂₅ concentrations is similar to the period between 13.8 ka
617 and 13.5 ka BP, which was characterized by ~~may point to perennial-cold~~ conditions and a ~~heavy-pronounced~~ -
618 potentially perennial - ice cover, the elevated TOC and biogenic opal values, as well as the presence of diatoms
619 associated with warm open ocean conditions at 0.5 ka BP, point to favorable ocean conditions. We hence relate
620 this drop in HBI concentrations to a shift in the diatom community rather than to an abrupt readvance of an ice
621 cover.

622 Late Holocene ocean temperature reconstructions for core PS97/072-1 display different patterns. Generally
623 increasing diatom-derived SSTs are only punctuated by a cooling event at 3.1 ka BP, while RI-OH' SOT remains
624 relatively constant with a very subtle cooling of ca. 0.2 °C between 1.5 ka and the present, which could be linked
625 to the slight decrease in summer insolation (Fig. 5a, b, c). The decrease in TEX₈₆^L SOT by about 1 °C between 4
626 ka and 3.3 ka BP in eastern Bransfield Strait is also depicted in the TEX₈₆^L data from the Palmer Deep core JPC10
627 (Fig. 5e, f; Etourneau et al., 2013). The following warming reflected in PS97/072-1 TEX₈₆^L SOT until ca. 2 ka
628 BP may relate to the establishment of open marine conditions fostering primary productivity at the Perseverance
629 Drift north of Joinville Island (northern tip of the AP) as a result of warm water intrusions (Kyrmanidou et al.,
630 2018). This warming is reversed by another cooling at about 2 ka BP - coincident with an abrupt temperature
631 increase of ca. 4 °C depicted in the ODP1089 TEX₈₆ SOT record in Palmer Deep (Fig. 5g; Shevenell et al., 2011).

632 The latter ~~This~~ warming is not displayed in the TEX₈₆^L data of the nearby JPC10 and we relate this contrast to the
633 different approaches used to determine SOT (*i.e.*, TEX₈₆ vs. TEX₈₆^L omitting the crenarchaeol regio-isomer, which
634 seems to be less important for membrane adaptation in polar waters; Kim et al., 2010).

635 Evidently, temperature trends at the AP in the Late Holocene are highly variable between different areas (Allen et
636 al., 2010; Barbara et al., 2016; Bárcena et al., 1998; Bentley et al., 2009; Etourneau et al., 2013; Mulvaney et al.,
637 2012; Shevenell et al., 2011) and this is likely associated with the complex oceanographic and atmospheric
638 settings. This heterogeneous pattern, however, contrasts with the currently observed large-scale ocean warming
639 along the AP driven by intrusions of ACC-derived warm CDW onto the continental shelf of the WAP (Couto et
640 al., 2017) and the NAP (Ruiz Barlett et al., 2018), as well as the overall loss of sea ice (Parkinson and Cavalieri,

Feldfunktion geändert

Feldfunktion geändert

Feldfunktion geändert

Feldfunktion geändert

Formatiert: Schriftart: Kursiv

641 2012), which supports the assumption that the recent changes impacting the AP already exceed natural variability.
642 conditions and the establishment of thick and/or compacted sea ice limiting the productivity of both phytoplankton
643 and also sea ice diatoms. This short period of sea ice growth may be related to the Little Ice Age (LIA), when
644 cooler conditions also triggered glacial readvance at the Antarctic Peninsula 500 years ago (e.g. Simms et al.,
645 2021). While a significant large pulse in sea ice export from the Arctic Ocean is proposed to have caused the LIA
646 cooling (Miles et al., 2020), knowledge about LIA sea ice conditions in the Southern Ocean is scarce and hence
647 inconclusive (Parkinson, 1990). The Neoglacial cooling as found in the JRI ice core, for example, is clearly
648 reflected in an increased sea ice cover at Palmer Deep since 2 ka BP (Fig. 4d, Etourneau et al., 2013) but this
649 record, however, contains no clear evidence for a further expansion of sea ice in response to the LIA. We conclude
650 that a comprehensive assessment of how Antarctic sea ice conditions changed during the LIA requires more studies
651 of well-dated and ideally higher resolved sediment records.
652 Similar to our sea ice signals, also the Late Holocene ocean temperature reconstructions display different patterns.
653 While RI-OH' SOT remains relatively stable, TEX₈₆⁺ indicates a cooling around 3 ka BP followed by a warming
654 until 1.5 ka BP and another cooling towards the top of the core. Diatom derived SSST also point to a cold period
655 around 3 ka BP immediately followed by peak a warming peak at ca. 2.5 ka BP. Evidently, temperature trends at
656 the WAP in the Late Holocene are highly variable between different areas (Allen et al., 2010; Barbara et al., 2016;
657 Bárcena et al., 1998; Bentley et al., 2009; Etourneau et al., 2013; Mulvaney et al., 2012; Shevenell et al., 2011)
658 and this may relate to the complex oceanographic and atmospheric settings. With regard to the diverging
659 temperature trends observed in sediment core PS97/072-1, we note that also inconsistencies between different
660 analytical approaches to reconstruct ocean temperatures need to be acknowledged and examined. As previously
661 stated, more information on the applicability and significance of GDGT derived ocean temperatures in polar
662 latitudes is needed.

663 5 Conclusions

664 We reconstructed the sea ice and climate development at the Northwest-AP since the last Deglacial using the
665 sediment core PS97/072-1 from the eastern Bransfield Strait. Pursuing a multi-proxy approach that focuses on
666 organic geochemical bulk and biomarker analyses, diatom assemblage studies and transfer functions as well as
667 IRD data, we identified different Deglacial and Holocene environmental conditions impacted by sea ice and
668 ocean temperature changes. In our multiproxy study we focused on the sea ice biomarker IPSO₂₅, the HBI-z-triene
669 representing open marine environments, and GDGTs for ocean temperature reconstructions. Diatom ecological
670 groups characteristic of sea ice or cold/warmer open ocean conditions were used, as well as diatom transfer

671 functions to reconstruct winter sea ice and summer sea surface temperature. Additional information was derived
672 from sedimentological records such as IRD and biogenic opal. Our results reveal the retreat of a perennial ice
673 cover floating ice shelf canopy after the ACR and an overall sea ice sea-ice reduction retreat and summer ocean
674 warming summer ocean temperatures during the Holocene. The late Deglacial from 13.89 ka to 11.7 ka BP was a
675 highly dynamic period: until 13.4 ka BP primary productivity the sedimentation of organic proxies was diminished
676 low due to a permanent ice cover during the ACR. The ACR terminated with a shift to slightly warming conditions
677 at 13 ka BP along with a reduction retreat in the length of the spring sea ice sea-ice season, which permitted
678 phytoplankton productivity at least during summer. The Early Holocene from 11.7 ka to 8.2 ka BP was
679 characterized by increasing summer ocean temperatures warming, further slightly decreasing (in terms of duration
680 and/or sea ice concentration) spring sea ice sea-ice cover in terms of duration and/or sea-ice concentration and
681 highly variable winter sea ice sea-ice cover. In the Middle Holocene from 8.2 ka to 4.2 ka BP, increased advection
682 of BSW and CDW led to a shortened sea ice sea-ice season (confined to winter and spring) sea ice coverage confined
683 to winter and spring season stable environmental conditions prevailed with elevated and rising summer ocean
684 temperatures fostering primary production, indicating and this period may be associated with the Middle Holocene
685 Climatic Optimum due to intervals of lower sea ice cover. In general, sea ice seasons were short and sea ice cover
686 was significantly greatly reduced to a minimum around 5.5 ka BP, even though high seasonal amplitudes and
687 short term, centennial changes in sea ice conditions occurred. During the Late Holocene, the core site experienced
688 a distinct fluctuations in variable WSI with concentrations shifting between 90% and 60% concentration, while
689 while PIPSO₂₅ values declined continuously suggesting a less intensive or shorter spring sea ice sea-ice covers spring
690 sea ice declined continuously. and a short term SSST cooling at 3 ka BP. Phytoplankton biomarkers as well as
691 sea ice proxies (IPSO₂₅₅, PIPSO₂₅₅, WSI) were lowest during the period coincident with the Little Ice Age which
692 we relate to the establishment of a multi-year sea ice cover. We note that GDGT-based TEX₈₆^L and RI-OH' SOTs
693 correspond to spring and summer insolation, respectively, which may explain the divergent trends displayed by
694 both SOT proxies. Clearly, while this observation may help with the interpretation of other Southern Ocean
695 GDGT-based temperature estimates and the reconstruction of seasonal SOT variability, more investigations into
696 the mechanisms driving GDGT synthesis in polar waters are needed.

697

698 **Data Availability**

699 All data mentioned in this paper will be available at the open access repository www.pangaea.de
700 (<https://doi.pangaea.de/10.1594/PANGAEA.952279>).

701 **Author contributions**

702 The study was conceived by MV and JM. Data collections and experimental investigations were done by MV
703 together with [CBL \(core description, sampling, diatoms, biogenic opal, age model\)](#), [PC \(diatoms\)](#), [AL \(age model,](#)
704 [diatoms\)](#), [OE \(diatom transfer function\)](#), [GM \(GDGTs \[PS97/072-1\]\(#\), ¹⁴C dating\)](#), [AVH \(\$\delta^{13}\text{C}\$ IPSO²⁵\)](#), [NL \(\$\delta^{13}\text{C}\$](#)
705 [TOC\)](#), [LLJ \(foraminifera, age model\)](#), [SMS \(age model, humming age\)](#), [CBL \(core description, sampling, diatoms,](#)
706 [biogenic opal, age model\)](#), [PC \(diatoms\)](#), [AL \(age model, diatoms\)](#), [OE \(diatom transfer function\)](#), [GM \(GDGTs](#)
707 [PS97/072-1, ¹⁴C dating\)](#), [AVH \(\$\delta^{13}\text{C}\$ IPSO²⁵\)](#), [NL \(\$\delta^{13}\text{C}\$ TOC\)](#), [J.Ee](#), DE and CE provided temperature and salinity
708 profiles near the study site. MV drafted the manuscript. All authors contributed to the interpretation and discussion
709 of the data and the finalization of this manuscript.

710

711 **Competing interests**

712 None of the authors have a conflict of interest.

713

714 **Acknowledgement**

715 We thank the captain, crew and chief scientist Frank Lamy of RV Polarstern cruise PS97. Denise Diekstall, Jens
716 Hefter, Alejandro Avila and Victor Acuña are thanked for their laboratory support. We thank Helge Arz for his
717 help with the age model. Simon Belt is acknowledged for providing the 7-HND internal standard for HBI
718 quantification. Financial support was provided through the Helmholtz Research grant VH-NG-1101. Partial
719 support from the Centers IDEAL (grant FONDAP 15150003) and COPAS [Sur-Austral \(grants AFB170006 and](#)
720 [FB210021\)](#), Chile, and the Spanish Ministry of Economy, Industry and Competitivity grants CTM2017-89711-
721 C2-½-P, co-funded by the European Union through FEDER funds, is acknowledged. We [appreciate](#)~~acknowledge~~
722 support by the Open Access Publication Funds of Alfred-Wegener-Institut Helmholtz-Zentrum für Polar- und
723 Meeresforschung.

724

725

726

727

| 728

| 729

| 730

| 731

| 732

| 733

| 734

- 735 **References**
- 736 [Abelmann, A., Gersonde, R., Cortese, G., Kuhn, G. and Smetacek, V.: Extensive phytoplankton blooms in the](#)
- 737 [Atlantic sector of the glacial Southern Ocean, *Paleoceanography*, 21\(1\), 1–9, doi:10.1029/2005PA001199, 2006.](#)
- 738 Alexander, V. and Niebauer, H. : Oceanography of the eastern Bering Sea ice-edge zone in spring, *Limn*, 26(6),
- 739 1111–1125 [online] Available from: <http://doi.wiley.com/10.1029/2007RG000250>, 1981.
- 740 Allen, C. S., Oakes-Fretwell, L., Anderson, J. B. and Hodgson, D. A.: A record of Holocene glacial and
- 741 oceanographic variability in Neny Fjord, Antarctic Peninsula, *The Holocene*, 20(4), 551–564,
- 742 doi:10.1177/0959683609356581, 2010.
- 743 Allison, I., Tivendale, C. M., Akerman, G. J., Tann, J. M. and Wills, R. H.: Seasonal Variations In The Surface
- 744 Energy Exchanges Over Antarctic Sea Ice and Coastal Waters, *Annals of Glaciology*, 3, 12–16,
- 745 doi:10.3189/S0260305500002445, 1982.
- 746 Anderson, R. F., Ali, S., Bradtmiller, L. I., Nielsen, S. H. H., Fleisher, M. Q., Anderson, B. E. and Burckle, L.
- 747 H.: Wind-Driven Upwelling in the Southern Ocean and the Deglacial Rise in Atmospheric CO₂, *Science*, 323,
- 748 1443–1448, doi:10.1126/science.1167441, 2009.
- 749 Armand, L. K. and Zielinski, U.: DIATOM SPECIES OF THE GENUS *RHIZOLENIA* FROM SOUTHERN
- 750 OCEAN SEDIMENTS: DISTRIBUTION AND TAXONOMIC NOTES, *Diatom Research*, 16(2), 259–294,
- 751 doi:10.1080/0269249X.2001.9705520, 2001.
- 752 Arrigo, K. R., Worthen, D. L., Lizotte, M. P., Dixon, P. and Dieckmann, G.: Primary Production in Antarctic Sea
- 753 Ice, *Science*, 276, 394–397, doi:10.1126/science.276.5311.394, 1997.
- 754 Barbara, L., Crosta, X., Schmidt, S. and Massé, G.: Diatoms and biomarkers evidence for major changes in sea
- 755 ice conditions prior the instrumental period in Antarctic Peninsula, *Quaternary Science Reviews*, 79, 99–110,
- 756 doi:10.1016/j.quascirev.2013.07.021, 2013.
- 757 Barbara, L., Crosta, X., Leventer, A., Schmidt, S., Etourneau, J., Domack, E. and Massé, G.: Environmental
- 758 responses of the Northeast Antarctic Peninsula to the Holocene climate variability, *Paleoceanography*, 31(1),
- 759 131–147, doi:10.1002/2015PA002785, 2016.
- 760 Bárcena, M. A., Gersonde, R., Ledesma, S., Fabrés, J., Calafat, A. M., Canals, M., Sierro, F. J. and Flores, J. A.:
- 761 Record of Holocene glacial oscillations in Bransfield Basin as revealed by siliceous microfossil assemblages,
- 762 *Antarctic Science*, 10(03), 269–285, doi:10.1017/S0954102098000364, 1998.
- 763 Belt, S. T.: Source-specific biomarkers as proxies for Arctic and Antarctic sea ice, *Organic Geochemistry*, 125,
- 764 277–298, doi:10.1016/j.orggeochem.2018.10.002, 2018.
- 765 Belt, S. T., Smik, L., Brown, T. A., Kim, J. H., Rowland, S. J., Allen, C. S., Gal, J. K., Shin, K. H., Lee, J. I. and

766 Taylor, K. W. R.: Source identification and distribution reveals the potential of the geochemical Antarctic sea ice
767 proxy IPSO25, *Nature Communications*, 7, 1–10, doi:10.1038/ncomms12655, 2016.

768 Belt, S. T. T., Brown, T. A. A., Ampel, L., Cabedo-Sanz, P., Fahl, K., Kocis, J. J. J., Massé, G., Navarro-
769 Rodriguez, A., Ruan, J. and Xu, Y.: An inter-laboratory investigation of the Arctic sea ice biomarker proxy IP25
770 in marine sediments: key outcomes and recommendations, *Climate of the Past*, 10(1), 155–166, doi:10.5194/cp-
771 10-155-2014, 2014.

772 Bentley, M. J., Hodgson, D. A., Smith, J. A., Cofaigh, C. ., Domack, E. W., Larter, R. D., Roberts, S. J.,
773 Brachfeld, S., Leventer, A., Hjort, C., Hillenbrand, C.-D. and Evans, J.: Mechanisms of Holocene
774 palaeoenvironmental change in the Antarctic Peninsula region, *The Holocene*, 19(1), 51–69,
775 doi:10.1177/0959683608096603, 2009.

776 Bentley, M. J., Ó Cofaigh, C., Anderson, J. B., Conway, H., Davies, B., Graham, A. G. C., Hillenbrand, C.-D.,
777 Hodgson, D. A., Jamieson, S. S. R., Larter, R. D., Mackintosh, A., Smith, J. A., Verleyen, E., Ackert, R. P., Bart,
778 P. J., Berg, S., Brunstein, D., Canals, M., Colhoun, E. A., Crosta, X., Dickens, W. A., Domack, E., Dowdeswell,
779 J. A., Dunbar, R., Ehrmann, W., Evans, J., Favier, V., Fink, D., Fogwill, C. J., Glasser, N. F., Gohl, K.,
780 Golledge, N. R., Goodwin, I., Gore, D. B., Greenwood, S. L., Hall, B. L., Hall, K., Hedding, D. W., Hein, A. S.,
781 Hocking, E. P., Jakobsson, M., Johnson, J. S., Jomelli, V., Jones, R. S., Klages, J. P., Kristoffersen, Y., Kuhn,
782 G., Leventer, A., Licht, K., Lilly, K., Lindow, J., Livingstone, S. J., Massé, G., McGlone, M. S., McKay, R. M.,
783 Melles, M., Miura, H., Mulvaney, R., Nel, W., Nitsche, F. O., O'Brien, P. E., Post, A. L., Roberts, S. J.,
784 Saunders, K. M., Selkirk, P. M., Simms, A. R., Spiegel, C., Stollendorf, T. D., Sugden, D. E., van der Putten, N.,
785 van Ommen, T., Verfaillie, D., Vyverman, W., Wagner, B., White, D. A., Witus, A. E. and Zwart, D.: A
786 community-based geological reconstruction of Antarctic Ice Sheet deglaciation since the Last Glacial Maximum,
787 *Quaternary Science Reviews*, 100(August), 1–9, doi:10.1016/j.quascirev.2014.06.025, 2014.

788 Blunier, T. and Brook, E. J.: Timing of millennial-scale climate change in antarctica and greenland during the
789 last glacial period, *Science*, 291(5501), 109–112, doi:10.1126/science.291.5501.109, 2001.

790 Boyer, T., Garcia, H. E., Locarnini, R. A., Zweng, M. M., Mishonov, A. V and Reagan, J. R.: *World Ocean*
791 *Atlas 2018.*, 2018.

792 Bracegirdle, T. J., Stephenson, D. B., Turner, J. and Phillips, T.: The importance of sea ice area biases in 21st
793 century multimodel projections of Antarctic temperature and precipitation, *Geophysical Research Letters*,
794 42(24), 10,832-10,839, doi:10.1002/2015GL067055, 2015.

795 Bracegirdle, T. J., Colleoni, F., Abram, N. J., Bertler, N. A. N., Dixon, D. A., England, M., Favier, V., Fogwill,
796 C. J., Fyfe, J. C., Goodwin, I., Goosse, H., Hobbs, W., Jones, J. M., Keller, E. D., Khan, A. L., Phipps, S. J.,

797 Raphael, M. N., Russell, J., Sime, L., Thomas, E. R., van den Broeke, M. R. and Wainer, I.: Back to the Future:
798 Using Long-Term Observational and Paleo-Proxy Reconstructions to Improve Model Projections of Antarctic
799 Climate, *Geosciences*, 9(6), 255, doi:10.3390/geosciences9060255, 2019.

800 Broecker, W. S.: Paleocean circulation during the Last Deglaciation: A bipolar seesaw?, *Paleoceanography*,
801 13(2), 119–121, doi:10.1029/97PA03707, 1998.

802 Buffen, A., Leventer, A., Rubin, A. and Hutchins, T.: Diatom assemblages in surface sediments of the
803 northwestern Weddell Sea, Antarctic Peninsula, *Marine Micropaleontology*, 62(1), 7–30,
804 doi:10.1016/J.MARMICRO.2006.07.002, 2007.

805 Butterworth, B. J. and Miller, S. D.: Air-sea exchange of carbon dioxide in the Southern Ocean and Antarctic
806 marginal ice zone, *Geophysical Research Letters*, 43(13), 7223–7230, doi:10.1002/2016GL069581, 2016.

807 Butzin, M., Köhler, P. and Lohmann, G.: Marine radiocarbon reservoir age simulations for the past 50,000 years,
808 *Geophysical Research Letters*, 44(16), 8473–8480, doi:10.1002/2017GL074688, 2017.

809 Cádiz Hernández, A.: Evidencia de cambios en la productividad marina a partir de testigos sedimentarios
810 recuperados en Bahía Fildes (Maxwell Bay) y Costa de Palmer, Península Antártica durante los últimos ~ 1000
811 años, Universidad de Valparaíso., 2019.

812 Canals, M. and Amblas, D.: Seafloor kettle holes in Orleans Trough, Bransfield Basin, Antarctic Peninsula,
813 *Geological Society, London, Memoirs*, 46(1), 313–314, doi:10.1144/M46.16, 2016a.

814 Canals, M. and Amblas, D.: The bundle: a mega-scale glacial landform left by an ice stream, Western Bransfield
815 Basin, *Geological Society, London, Memoirs*, 46(1), 177–178, doi:10.1144/M46.157, 2016b.

816 Canals, M., Amblas, D. and Casamor, J. L.: Cross-shelf troughs in Central Bransfield Basin, Antarctic Peninsula,
817 *Geological Society, London, Memoirs*, 46(1), 171–172, doi:10.1144/M46.138, 2016.

818 Cárdenas, P., Lange, C. B., Vernet, M., Esper, O., Srain, B., Vorrath, M.-E. M.-E., Ehrhardt, S., Müller, J.,
819 Kuhn, G., Arz, H. W. H. W. H. W., Lembke-Jene, L., Lamy, F. and Paola Cárdenas, Carina B. Lange, Maria
820 Vernet, Oliver Esper, Benjamin Srain, Maria-Elena Vorrath, Sophie Ehrhardt, Juliane Müller, Gerhard Kuhn,
821 Helge W. Arz, Lester Lembke-Jene, F. L.: Biogeochemical proxies and diatoms in surface sediments across the
822 Drake Passage reflect oceanic domains and frontal systems in the region, *Progress in Oceanography*, 174, 72–88,
823 doi:10.1016/j.pocean.2018.10.004, 2019.

824 Carrasco, J. F., Bozkurt, D. and Cordero, R. R.: A review of the observed air temperature in the Antarctic
825 Peninsula. Did the warming trend come back after the early 21st hiatus?, *Polar Science*, 28, 100653,
826 doi:10.1016/j.polar.2021.100653, 2021.

827 Cavalieri, D. J., Parkinson, C. L., Gloersen, P. and Zwally, H. J.: Sea Ice Concentrations from Nimbus-7 SMMR

828 and DMSP SSM/I-SSMIS Passive Microwave Data, Version 1, Boulder, Colorado USA,
829 doi:10.5067/8GQ8LZQVL0VL, 1996.

830 Chisholm, S. W.: Stirring times in the Southern Ocean, *Nature*, 407(6805), 685–686, doi:10.1038/35037696,
831 2000.

832 Clark, P. U., Shakun, J. D., Baker, P. A., Bartlein, P. J., Brewer, S., Brook, E., Carlson, A. E., Cheng, H.,
833 Kaufman, D. S., Liu, Z., Marchitto, T. M., Mix, A. C., Morrill, C., Otto-Bliesner, B. L., Pahnke, K., Russell, J.
834 M., Whitlock, C., Adkins, J. F., Blois, J. L., Clark, J., Colman, S. M., Curry, W. B., Flower, B. P., He, F.,
835 Johnson, T. C., Lynch-Stieglitz, J., Markgraf, V., McManus, J., Mitrovica, J. X., Moreno, P. I. and Williams, J.
836 W.: Global climate evolution during the last deglaciation, *Proceedings of the National Academy of Sciences*,
837 109(19), E1134–E1142, doi:10.1073/pnas.1116619109, 2012.

838 Collares, L. L., Mata, M. M., Kerr, R., Arigony-Neto, J. and Barbat, M. M.: Iceberg drift and ocean circulation
839 in the northwestern Weddell Sea, Antarctica, *Deep Sea Research Part II: Topical Studies in Oceanography*,
840 149(January 2019), 10–24, doi:10.1016/j.dsr2.2018.02.014, 2018.

841 Cook, A. J., Holland, P. R., Meredith, M. P., Murray, T., Luckman, A. and Vaughan, D. G.: Ocean forcing of
842 glacier retreat in the western Antarctic Peninsula, *Science*, 353(6296), 283–286, doi:10.1126/science.aae0017,
843 2016.

844 Couto, N., Martinson, D. G., Kohut, J. and Schofield, O.: Distribution of Upper Circumpolar Deep Water on the
845 warming continental shelf of the West Antarctic Peninsula, *Journal of Geophysical Research: Oceans*, 122(7),
846 5306–5315, doi:10.1002/2017JC012840, 2017.

847 Crosta, X., Kohfeld, K. E., Bostock, H. C., Chadwick, M., Du Vivier, A., Esper, O., Etourneau, J., Jones, J.,
848 Leventer, A., Müller, J., Rhodes, R. H., Allen, C. S., Ghadi, P., Lamping, N., Lange, C. B., Lawler, K.-A., Lund,
849 D., Marzocchi, A., Meissner, K. J., Menviel, L., Nair, A., Patterson, M., Pike, J., Prebble, J. G., Riesselman, C.,
850 Sadatzki, H., Sime, L. C., Shukla, S. K., Thöle, L., Vorrath, M.-E., Xiao, W. and Yang, J.: Antarctic sea ice over
851 the past 130,000 years, Part I: A review of what proxy records tell us, *EGUsphere* [preprint],
852 doi:10.5194/egusphere-2022-99, 2022.

853 Denis, D., Crosta, X., Barbara, L., Massé, G., Renssen, H., Ther, O. and Giraudeau, J.: Sea ice and wind
854 variability during the Holocene in East Antarctica: insight on middle–high latitude coupling, *Quaternary Science*
855 *Reviews*, 29(27–28), 3709–3719, doi:10.1016/J.QUASCIREV.2010.08.007, 2010.

856 Domack, E., Leventer, A., Dunbar, R., Taylor, F., Brachfeld, S. and Sjunneskogs, C.: Chronology of the Palmer
857 Deep site, Antarctic Peninsula: a Holocene palaeoenvironmental reference for the circum-Antarctic, *The*
858 *Holocene*, 11(1), 1–9, doi:10.1191/095968301673881493, 2001.

859 Domack, E. W.: A Synthesis for Site 1098: Palmer Deep, in Proceedings of the Ocean Drilling Program, 178
860 Scientific Results, Ocean Drilling Program., 2002.

861 Ducklow, H. W., Erickson, M., Kelly, J., Montes-Hugo, M., Ribic, C. A., Smith, R. C., Stammerjohn, S. E. and
862 Karl, D. M.: Particle export from the upper ocean over the continental shelf of the west Antarctic Peninsula: A
863 long-term record, 1992–2007, Deep Sea Research Part II: Topical Studies in Oceanography, 55(18–19), 2118–
864 2131, doi:10.1016/j.dsr2.2008.04.028, 2008.

865 EPICA Community Members: Eight glacial cycles from an Antarctic ice core, Nature, 429(6992), 623–628,
866 doi:10.1038/nature02599, 2004.

867 EPICA Community Members: One-to-one coupling of glacial climate variability in Greenland and Antarctica,
868 Nature, 444(7116), 195–198, doi:10.1038/nature05301, 2006.

869 Escutia, C., DeConto, R., Dunbar, R., De Santis, L., Shevenell, A. and Nash, T.: Keeping an Eye on Antarctic
870 Ice Sheet Stability, Oceanography, 32(1), 32–46, doi:10.5670/oceanog.2019.117, 2019.

871 Esper, O. and Gersonde, R.: New tools for the reconstruction of Pleistocene Antarctic sea ice, Palaeogeography,
872 Palaeoclimatology, Palaeoecology, 399, 260–283, doi:10.1016/J.PALAEO.2014.01.019, 2014a.

873 Esper, O. and Gersonde, R.: Quaternary surface water temperature estimations: New diatom transfer functions
874 for the Southern Ocean, Palaeogeography, Palaeoclimatology, Palaeoecology, 414, 1–19,
875 doi:10.1016/J.PALAEO.2014.08.008, 2014b.

876 Esper, O., Gersonde, R. and Kadagies, N.: Diatom distribution in southeastern Pacific surface sediments and
877 their relationship to modern environmental variables, Palaeogeography, Palaeoclimatology, Palaeoecology,
878 287(1–4), 1–27, doi:10.1016/J.PALAEO.2009.12.006, 2010.

879 Etourneau, J., Collins, L. G., Willmott, V., Kim, J. H., Barbara, L., Leventer, A., Schouten, S., Sinninghe
880 Damsté, J. S., Bianchini, A., Klein, V., Crosta, X. and Massé, G.: Holocene climate variations in the western
881 Antarctic Peninsula: Evidence for sea ice extent predominantly controlled by changes in insolation and ENSO
882 variability, Climate of the Past, 9(4), 1431–1446, doi:10.5194/cp-9-1431-2013, 2013.

883 Etourneau, J., Sgubin, G., Crosta, X., Swingedouw, D., Willmott, V., Barbara, L., Houssais, M. N., Schouten, S.,
884 Damsté, J. S. S., Goosse, H., Escutia, C., Crespin, J., Massé, G. and Kim, J. H.: Ocean temperature impact on ice
885 shelf extent in the eastern Antarctic Peninsula, Nature Communications, 10(1), 8–15, doi:10.1038/s41467-018-
886 08195-6, 2019.

887 Fietz, S., Hugué, C., Rueda, G., Hambach, B. and Rosell-Melé, A.: Hydroxylated isoprenoidal GDGTs in the
888 Nordic Seas, Marine Chemistry, 152, 1–10, doi:10.1016/j.marchem.2013.02.007, 2013.

889 Fischer, H., Fundel, F., Ruth, U., Twarloh, B., Wegner, A., Udisti, R., Becagli, S., Castellano, E., Morganti, A.,

890 Severi, M., Wolff, E., Littot, G., Röthlisberger, R., Mulvaney, R., Hutterli, M. A., Kaufmann, P., Federer, U.,
891 Lambert, F., Bigler, M., Hansson, M., Jonsell, U., de Angelis, M., Boutron, C., Siggaard-Andersen, M.-L.,
892 Steffensen, J. P., Barbante, C., Gaspari, V., Gabrielli, P. and Wagenbach, D.: Reconstruction of millennial
893 changes in dust emission, transport and regional sea ice coverage using the deep EPICA ice cores from the
894 Atlantic and Indian Ocean sector of Antarctica, *Earth and Planetary Science Letters*, 260(1–2), 340–354,
895 doi:10.1016/j.epsl.2007.06.014, 2007.

896 Fletcher, M.-S., Pedro, J., Hall, T., Mariani, M., Alexander, J. A., Beck, K., Blaauw, M., Hodgson, D. A.,
897 Heijnis, H., Gadd, P. S. and Lise-Pronovost, A.: Northward shift of the southern westerlies during the Antarctic
898 Cold Reversal, *Quaternary Science Reviews*, 271, 107189, doi:10.1016/j.quascirev.2021.107189, 2021.

899 Gersonde, R. and Zielinski, U.: The reconstruction of late Quaternary Antarctic sea-ice distribution — the use of
900 diatoms as a proxy for sea-ice, , 162, 263–286, doi:10.1016/S0031-0182(00)00131-0, 2000.

901 Gersonde, R., Crosta, X., Abelmann, A. and Armand, L.: Sea-surface temperature and sea ice distribution of the
902 Southern Ocean at the EPILOG Last Glacial Maximum—a circum-Antarctic view based on siliceous microfossil
903 records, *Quaternary Science Reviews*, 24(7–9), 869–896, doi:10.1016/J.QUASCIREV.2004.07.015, 2005.

904 Gloersen, P., Campbell, W. J., Cavalieri, D. J., Comiso, J. C., Parkinson, C. L. and Zwally, H. J.: Arctic and
905 antarctic sea ice, 1978, *Annals of Glaciology*, 17, 149–154, 1993.

906 Gonçalves-Araujo, R., de Souza, M. S., Tavano, V. M. and Garcia, C. A. E.: Influence of oceanographic features
907 on spatial and interannual variability of phytoplankton in the Bransfield Strait, Antarctica, *Journal of Marine*
908 *Systems*, 142, 1–15, doi:10.1016/J.JMARSYS.2014.09.007, 2015.

909 Gottschalk, J., Michel, E., Thöle, L. M., Studer, A. S., Hasenfratz, A. P., Schmid, N., Butzin, M., Mazaud, A.,
910 Martínez-García, A., Szidat, S. and Jaccard, S. L.: Glacial heterogeneity in Southern Ocean carbon storage
911 abated by fast South Indian deglacial carbon release, *Nature Communications*, 11(1), 6192, doi:10.1038/s41467-
912 020-20034-1, 2020.

913 Green, R. A., Menviel, L., Meissner, K. J., Crosta, X., Chandan, D., Lohmann, G., Peltier, W. R., Shi, X. and
914 Zhu, J.: Evaluating seasonal sea-ice cover over the Southern Ocean at the Last Glacial Maximum, *Climate of the*
915 *Past*, 18(4), 845–862, doi:10.5194/cp-18-845-2022, 2022.

916 Han, Z., Hu, C., Sun, W., Zhao, J., Pan, J., Fan, G. and Zhang, H.: Characteristics of particle fluxes in the Prydz
917 Bay polynya, Eastern Antarctica, *Science China Earth Sciences*, 62(4), 657–670, doi:10.1007/s11430-018-9285-
918 6, 2019.

919 Hellmer, H. H., Kauker, F., Timmermann, R., Determann, J. and Rae, J.: Twenty-first-century warming of a
920 large Antarctic ice-shelf cavity by a redirected coastal current, *Nature*, 485(7397), 225–228,

921 doi:10.1038/nature11064, 2012.

922 Heroy, D. C., Sjunneskog, C. and Anderson, J. B.: Holocene climate change in the Bransfield Basin, Antarctic
923 Peninsula: evidence from sediment and diatom analysis, *Antarctic Science*, 20(01), 69–87,
924 doi:10.1017/S0954102007000788, 2008.

925 Hillaire-Marcel, C. and de Vernal, A.: *Proxies in Late Cenozoic Paleoceanography*, edited by C. Hillaire-Marcel
926 and A. de Vernal, Elsevier, Amsterdam., 2007.

927 Hofmann, E. E., Klinck, J. M., Lascara, C. M. and Smith, D. A.: Water mass distribution and circulation west of
928 the Antarctic Peninsula and including Bransfield Strait, pp. 61–80, American Geophysical Union (AGU)., 1996.

929 Hopmans, E. C., Weijers, J. W. H., Schefuß, E., Herfort, L., Sinninghe Damsté, J. S. and Schouten, S.:
930 Variability in the Benguela Current upwelling system over the past 70,000 years, *Earth and Planetary Science*
931 *Letters*, 224(1–2), 107–116, doi:10.1016/j.epsl.2004.05.012, 2004.

932 Huss, M. and Farinotti, D.: A high-resolution bedrock map for the Antarctic Peninsula, *The Cryosphere*, 8(4),
933 1261–1273, doi:10.5194/tc-8-1261-2014, 2014.

934 Ingólfsson, Ó., Hjort, C. and Humlum, O.: Glacial and Climate History of the Antarctic Peninsula since the Last
935 Glacial Maximum, *Arctic, Antarctic, and Alpine Research*, 35(2), 175–186, doi:10.1657/1523-
936 0430(2003)035[0175:GACHOT]2.0.CO;2, 2003.

937 IPCC: Summary for Policymakers, in *Climate Change 2021_ The Physical Science Basis. Contribution of*
938 *working Group I to the Sixth Assessment Report of the Intergovernmental Panel on Climate Change*, edited by
939 V. Masson-Delmotte, P. Zhai, H.-O. Pörtner, D. Roberts, J. Skea, P. R. Shukla, A. Pirani, W. Moufouma-Okia,
940 C. Péan, R. Pidcock, S. Connors, J. B. R. Matthews, Y. Chen, X. Zhou, M. I. Gomis, E. Lonnoy, T. Maycock,
941 M. Tignor, and T. Waterfield, p. 32, Cambridge University Press., 2021.

942 Jones, R. S., Johnson, J. S., Lin, Y., Mackintosh, A. N., Sefton, J. P., Smith, J. A., Thomas, E. R. and
943 Whitehouse, P. L.: Stability of the Antarctic Ice Sheet during the pre-industrial Holocene, *Nature Reviews Earth*
944 *& Environment*, 3(8), 500–515, doi:10.1038/s43017-022-00309-5, 2022.

945 Jouzel, J., Vaikmae, R., Petit, J. R., Martin, M., Duclos, Y., Stievenard, M., Lorius, C., Toots, M., Mélières, M.
946 A., Burckle, L. H., Barkov, N. I. and Kotlyakov, V. M.: The two-step shape and timing of the last deglaciation in
947 Antarctica, *Climate Dynamics*, 11(3), 151–161, doi:10.1007/BF00223498, 1995.

948 Kalanetra, K. M., Bano, N. and Hollibaugh, J. T.: Ammonia-oxidizing Archaea in the Arctic Ocean and
949 Antarctic coastal waters, *Environmental Microbiology*, 11(9), 2434–2445, doi:10.1111/j.1462-
950 2920.2009.01974.x, 2009.

951 Kim, D., Kim, D. Y., Kim, Y. J., Kang, Y. C. and Shim, J.: Downward fluxes of biogenic material in Bransfield

952 Strait, Antarctica, *Antarctic Science*, 16(3), 227–237, doi:10.1017/S0954102004002032, 2004.

953 Kim, J.-H., van der Meer, J., Schouten, S., Helmke, P., Willmott, V., Sangiorgi, F., Koç, N., Hopmans, E. C. and
954 Damsté, J. S. S.: New indices and calibrations derived from the distribution of crenarchaeal isoprenoid tetraether
955 lipids: Implications for past sea surface temperature reconstructions, *Geochimica et Cosmochimica Acta*, 74(16),
956 4639–4654, doi:10.1016/j.gca.2010.05.027, 2010.

957 Kim, J.-H., Crosta, X., Willmott, V., Renssen, H., Bonnin, J., Helmke, P., Schouten, S. and Sinninghe Damsté, J.
958 S.: Holocene subsurface temperature variability in the eastern Antarctic continental margin, *Geophysical*
959 *Research Letters*, 39(6), doi:10.1029/2012GL051157, 2012.

960 Klunder, M. B., Laan, P., De Baar, H. J. W., Middag, R., Neven, I. and Van Ooijen, J.: Dissolved Fe across the
961 Weddell Sea and Drake Passage: impact of DFe on nutrient uptake, *Biogeosciences*, 11(3), 651–669,
962 doi:10.5194/bg-11-651-2014, 2014.

963 Kyrmanidou, A., Vadman, K. J., Ishman, S. E., Leventer, A., Brachfeld, S., Domack, E. W. and Wellner, J. S.:
964 Late Holocene oceanographic and climatic variability recorded by the Perseverance Drift, northwestern Weddell
965 Sea, based on benthic foraminifera and diatoms, *Marine Micropaleontology*, 141, 10–22,
966 doi:10.1016/j.marmicro.2018.03.001, 2018.

967 Lamping, N., Müller, J., Esper, O., Hillenbrand, C., Smith, J. A. and Kuhn, G.: Highly branched isoprenoids
968 reveal onset of deglaciation followed by dynamic sea-ice conditions in the western Amundsen Sea, Antarctica,
969 *Quaternary Science Reviews*, 228, 106103, doi:10.1016/j.quascirev.2019.106103, 2020.

970 Lamping, N., Müller, J., Hefter, J., Mollenhauer, G., Haas, C., Shi, X., Vorrath, M.-E., Lohmann, G. and
971 Hillenbrand, C.-D.: Evaluation of lipid biomarkers as proxies for sea ice and ocean temperatures along the
972 Antarctic continental margin, *Climate of the Past*, 17(5), 2305–2326, doi:10.5194/cp-17-2305-2021, 2021.

973 Lamy, F.: The expedition PS97 of the research vessel POLARSTERN to the Drake Passage in 2016, *Reports on*
974 *Polar and Marine Research*, 7⁰¹, 1–571, doi:10.2312/BzPM_0702_2016, 2016.

975 Lamy, F., Kaiser, J., Arz, H. W., Hebbeln, D., Ninnemann, U., Timm, O., Timmermann, A. and Toggweiler, J.
976 R.: Modulation of the bipolar seesaw in the Southeast Pacific during Termination 1, *Earth and Planetary Science*
977 *Letters*, 259(3–4), 400–413, doi:10.1016/j.epsl.2007.04.040, 2007.

978 Lhardy, F., Bouttes, N., Roche, D. M., Crosta, X., Waelbroeck, C. and Paillard, D.: Impact of Southern Ocean
979 surface conditions on deep ocean circulation during the LGM: a model analysis, *Climate of the Past*, 17(3),
980 1139–1159, doi:10.5194/cp-17-1139-2021, 2021.

981 Liu, R., Han, Z., Zhao, J., Zhang, H., Li, D., Ren, J., Pan, J. and Zhang, H.: Distribution and source of glycerol
982 dialkyl glycerol tetraethers (GDGTs) and the applicability of GDGT-based temperature proxies in surface

983 sediments of Prydz Bay, East Antarctica, *Polar Research*, 39, doi:10.33265/polar.v39.3557, 2020.

984 Locarnini, M., Mishonov, A., Baranova, O., Boyer, T., Zweng, M., Garcia, H., Reagan, J., Seidov, D., Weathers,
985 K., Paver, C. and Smolyar, I.: *World Ocean Atlas 2018, Volume 1: Temperature*. [online] Available from:
986 <https://archimer.ifremer.fr/doc/00651/76338/>, 2018.

987 Lü, X., Liu, X. L., Elling, F. J., Yang, H., Xie, S., Song, J., Li, X., Yuan, H., Li, N. and Hinrichs, K. U.:
988 Hydroxylated isoprenoid GDGTs in Chinese coastal seas and their potential as a paleotemperature proxy for
989 mid-to-low latitude marginal seas, *Organic Geochemistry*, 89–90, 31–43,
990 doi:10.1016/j.orggeochem.2015.10.004, 2015.

991 Martinson, D. G. and McKee, D. C.: Transport of warm Upper Circumpolar Deep Water onto the western
992 Antarctic Peninsula continental shelf, *Ocean Science*, 8(4), 433–442, doi:10.5194/os-8-433-2012, 2012.

993 Massé, G., Belt, S. T., Crosta, X., Schmidt, S., Snape, I., Thomas, D. N. and Rowland, S. J.: Highly branched
994 isoprenoids as proxies for variable sea ice conditions in the Southern Ocean, *Antarctic Science*, 23(05), 487–498,
995 doi:10.1017/S0954102011000381, 2011.

996 McClymont, E. L., Bentley, M. J., Hodgson, D. A., Spencer-Jones, C. L., Wardley, T., West, M. D., Croudace, I.
997 W., Berg, S., Gröcke, D. R., Kuhn, G., Jamieson, S. S. R., Sime, L. and Phillips, R. A.: Summer sea-ice
998 variability on the Antarctic margin during the last glacial period reconstructed from snow petrel (*Pagodroma
999 nivea*) stomach-oil deposits, *Climate of the Past*, 18(2), 381–403, doi:10.5194/cp-18-381-2022, 2022.

1000 Meredith, M. P. and King, J. C.: Rapid climate change in the ocean west of the Antarctic Peninsula during the
1001 second half of the 20th century, *Geophysical Research Letters*, 32(19), 1–5, doi:10.1029/2005GL024042, 2005.

1002 Milliken, K. T., Anderson, J. B., Wellner, J. S., Bohaty, S. M. and Manley, P. L.: High-resolution Holocene
1003 climate record from Maxwell Bay, South Shetland Islands, Antarctica, *Geological Society of America Bulletin*,
1004 121(11–12), 1711–1725, doi:10.1130/B26478.1, 2009.

1005 Minzoni, R. T., Anderson, J. B., Fernandez, R. and Wellner, J. S.: Marine record of Holocene climate, ocean,
1006 and cryosphere interactions: Herbert Sound, James Ross Island, Antarctica, *Quaternary Science Reviews*, 129,
1007 239–259, doi:10.1016/j.quascirev.2015.09.009, 2015.

1008 Mollenhauer, G., Grotheer, H., Gentz, T., Bonk, E. and Hefter, J.: Standard operation procedures and
1009 performance of the MICADAS radiocarbon laboratory at Alfred Wegener Institute (AWI), Germany, *Nuclear
1010 Instruments and Methods in Physics Research Section B: Beam Interactions with Materials and Atoms*, 496, 45–
1011 51, doi:10.1016/j.nimb.2021.03.016, 2021.

1012 Morigi, C., Capotondi, L., Giglio, F., Langone, L., Brilli, M., Turi, B. and Ravaioli, M.: A possible record of the
1013 Younger Dryas event in deep-sea sediments of the Southern Ocean (Pacific sector), in *Palaeogeography*,

1014 Palaeoclimatology, Palaeoecology, vol. 198, pp. 265–278, Elsevier B.V., 2003.

1015 Mortlock, R. A. and Froelich, P. N.: A simple method for the rapid determination of biogenic opal in pelagic
1016 marine sediments, *Deep Sea Research Part A, Oceanographic Research Papers*, 36(9), 1415–1426,
1017 doi:10.1016/0198-0149(89)90092-7, 1989.

1018 Müller, J., Wagner, A., Fahl, K., Stein, R., Prange, M. and Lohmann, G.: Towards quantitative sea ice
1019 reconstructions in the northern North Atlantic: A combined biomarker and numerical modelling approach, *Earth
1020 and Planetary Science Letters*, 306(3–4), 137–148, doi:10.1016/J.EPSL.2011.04.011, 2011.

1021 Müller, P. J. and Schneider, R.: An automated leaching method for the determination of opal in sediments and
1022 particulate matter, *Deep-Sea Research Part I*, 40(3), 425–444, doi:https://doi.org/10.1016/0967-0637(93)90140-
1023 X, 1993.

1024 Mulvaney, R., Abram, N. J., Hindmarsh, R. C. A., Arrowsmith, C., Fleet, L., Triest, J., Sime, L. C., Alemany, O.
1025 and Foord, S.: Recent Antarctic Peninsula warming relative to Holocene climate and ice-shelf history, *Nature*,
1026 489(7414), 141–144, doi:10.1038/nature11391, 2012.

1027 Murray, A. E., Preston, C. M., Massana, R., Taylor, L. T., Blakis, A., Wu, K. and DeLong, E. F.: Seasonal and
1028 Spatial Variability of Bacterial and Archaeal Assemblages in the Coastal Waters near Anvers Island, Antarctica,
1029 *Applied and Environmental Microbiology*, 64(7), 2585–2595, doi:10.1128/AEM.64.7.2585-2595.1998, 1998.

1030 Nicholls, K. W., Østerhus, S., Makinson, K., Gammelsrød, T. and Fahrback, E.: Ice-ocean processes over the
1031 continental shelf of the southern Weddell Sea, Antarctica: A review, *Reviews of Geophysics*, 47(3), RG3003,
1032 doi:10.1029/2007RG000250, 2009.

1033 Ó Cofaigh, C., Davies, B. J., Livingstone, S. J., Smith, J. A., Johnson, J. S., Hocking, E. P., Hodgson, D. A.,
1034 Anderson, J. B., Bentley, M. J., Canals, M., Domack, E., Dowdeswell, J. A., Evans, J., Glasser, N. F.,
1035 Hillenbrand, C.-D., Larter, R. D., Roberts, S. J. and Simms, A. R.: Reconstruction of ice-sheet changes in the
1036 Antarctic Peninsula since the Last Glacial Maximum, *Quaternary Science Reviews*, 100, 87–110,
1037 doi:10.1016/j.quascirev.2014.06.023, 2014.

1038 Oksanen, J., Blanchet, F. G., Kindt, R., Legendre, P., Minchin, P. R., O'Hara, R. B., Simpson, G. L., Solymos,
1039 P., Stevens, M. H. H. and Wagner, H.: *Vegan: Community Ecology Package (R Package Version 2.0-3)*, 2012.

1040 Parkinson, C. L. and Cavalieri, D. J.: Antarctic sea ice variability and trends, 1979–2010, *The Cryosphere*, 6,
1041 871–880, doi:10.5194/tc-6-871-2012, 2012.

1042 Pedro, J. B., Bostock, H. C., Bitz, C. M., He, F., Vandergoes, M. J., Steig, E. J., Chase, B. M., Krause, C. E.,
1043 Rasmussen, S. O., Markle, B. R. and Cortese, G.: The spatial extent and dynamics of the Antarctic Cold
1044 Reversal, *Nature Geoscience*, 9(1), 51–55, doi:10.1038/ngeo2580, 2016.

1045 QGIS, D. T.: QGIS Geographic Information System, [online] Available from: <http://qgis.osgeo.org>, 2018.

1046 R Core Team: R: a Language and Environment for Statistical Computing, R Foundation for Statistical
 1047 computing, Vienna., 2012.

1048 Reimer, P. J., Austin, W. E. N., Bard, E., Bayliss, A., Blackwell, P. G., Bronk Ramsey, C., Butzin, M., Cheng,
 1049 H., Edwards, R. L., Friedrich, M., Grootes, P. M., Guilderson, T. P., Hajdas, I., Heaton, T. J., Hogg, A. G.,
 1050 Hughen, K. A., Kromer, B., Manning, S. W., Muscheler, R., Palmer, J. G., Pearson, C., van der Plicht, J.,
 1051 Reimer, R. W., Richards, D. A., Scott, E. M., Southon, J. R., Turney, C. S. M., Wacker, L., Adolphi, F.,
 1052 Büntgen, U., Capano, M., Fahrni, S. M., Fogtmann-Schulz, A., Friedrich, R., Köhler, P., Kudsk, S., Miyake, F.,
 1053 Olsen, J., Reinig, F., Sakamoto, M., Sookdeo, A. and Talamo, S.: The IntCal20 Northern Hemisphere
 1054 Radiocarbon Age Calibration Curve (0–55 cal kBP), *Radiocarbon*, 62(4), 725–757, doi:10.1017/RDC.2020.41,
 1055 2020.

1056 Reynolds, R. W., Rayner, N. A., Smith, T. M., Stokes, D. C., Wang, W., Reynolds, R. W., Rayner, N. A., Smith,
 1057 T. M., Stokes, D. C. and Wang, W.: An Improved In Situ and Satellite SST Analysis for Climate, *Journal of*
 1058 *Climate*, 15(13), 1609–1625, doi:10.1175/1520-0442(2002)015<1609:AIISAS>2.0.CO;2, 2002.

1059 Reynolds, R. W., Smith, T. M., Liu, C., Chelton, D. B., Casey, K. S., Schlax, M. G., Reynolds, R. W., Smith, T.
 1060 M., Liu, C., Chelton, D. B., Casey, K. S. and Schlax, M. G.: Daily High-Resolution-Blended Analyses for Sea
 1061 Surface Temperature, *Journal of Climate*, 20(22), 5473–5496, doi:10.1175/2007JCLI1824.1, 2007.

1062 Rignot, E., Mouginot, J., Scheuchl, B., van den Broeke, M., van Wessem, M. J. and Morlighem, M.: Four
 1063 decades of Antarctic Ice Sheet mass balance from 1979–2017, *Proceedings of the National Academy of*
 1064 *Sciences*, 116(4), 1095–1103, doi:10.1073/pnas.1812883116, 2019.

1065 Roche, D. M., Crosta, X. and Renssen, H.: Evaluating Southern Ocean sea-ice for the Last Glacial Maximum
 1066 and pre-industrial climates: PMIP-2 models and data evidence, *Quaternary Science Reviews*, 56, 99–106,
 1067 doi:10.1016/j.quascirev.2012.09.020, 2012.

1068 Ronge, T. A., Lippold, J., Geibert, W., Jaccard, S. L., Mieruch-Schnülle, S., Siefke, F. and Tiedemann, R.:
 1069 Deglacial patterns of South Pacific overturning inferred from 231Pa and 230Th, *Scientific Reports*, 11(1),
 1070 doi:10.1038/s41598-021-00111-1, 2021.

1071 Roseby, Z. A., Smith, J. A., Hillenbrand, C.-D., Cartigny, M. J. B., Rosenheim, B. E., Hogan, K. A., Allen, C.
 1072 S., Leventer, A., Kuhn, G., Ehrmann, W. and Larter, R. D.: History of Anvers-Hugo Trough, western Antarctic
 1073 Peninsula shelf, since the Last Glacial Maximum. Part I: Deglacial history based on new sedimentological and
 1074 chronological data, *Quaternary Science Reviews*, 291, 107590, doi:10.1016/j.quascirev.2022.107590, 2022.

1075 Ruiz Barlett, E. M., Tosonotto, G. V., Piola, A. R., Sierra, M. E. and Mata, M. M.: On the temporal variability of

1076 intermediate and deep waters in the Western Basin of the Bransfield Strait, *Deep Sea Research Part II: Topical*
1077 *Studies in Oceanography*, 149, 31–46, doi:10.1016/j.dsr2.2017.12.010, 2018.

1078 Sangrà, P., Gordo, C., Hernández-Arencibia, M., Marrero-Díaz, A., Rodríguez-Santana, A., Stegner, A.,
1079 Martínez-Marrero, A., Pelegrí, J. L. and Pichon, T.: The Bransfield current system, *Deep Sea Research Part I:*
1080 *Oceanographic Research Papers*, 58(4), 390–402, doi:10.1016/J.DSR.2011.01.011, 2011.

1081 Sangrà, P., Stegner, A., Hernández-Arencibia, M., Marrero-Díaz, Á., Salinas, C., Aguiar-González, B.,
1082 Henríquez-Pastene, C. and Mouriño-Carballido, B.: The Bransfield Gravity Current, *Deep-Sea Research Part I:*
1083 *Oceanographic Research Papers*, 119(November 2016), 1–15, doi:10.1016/j.dsr.2016.11.003, 2017.

1084 Scherer, R. P.: A new method for the determination of absolute abundance of diatoms and other silt-sized
1085 sedimentary particles, *Journal of Paleolimnology*, 12(2), 171–179, doi:10.1007/BF00678093, 1994.

1086 Schlüter, M. and Rickert, D.: Effect of pH on the measurement of biogenic silica, *Marine Chemistry*, 63(1–2),
1087 81–92, doi:10.1016/S0304-4203(98)00052-8, 1998.

1088 Schofield, O., Brown, M., Kohut, J., Nardelli, S., Saba, G., Waite, N. and Ducklow, H.: Changes in the upper
1089 ocean mixed layer and phytoplankton productivity along the West Antarctic Peninsula, *Philosophical*
1090 *Transactions of the Royal Society A: Mathematical, Physical and Engineering Sciences*, 376(2122),
1091 doi:10.1098/rsta.2017.0173, 2018.

1092 Schrader, H. and Gersonde, R.: Diatoms and silicoflagellates, in *Micropaleontological Methods and Techniques*
1093 - An Exercise on an Eight Meter Section of the Lower Pliocene of Capo Rossello, Sicily, Utrecht
1094 *Micropaleontological Bulletins*, vol. 17, edited by W. J. Zachariasse, W. R. Riedel, A. Sanfilippo, R. R. Schmidt,
1095 M. J. Brotsma, H. J. Schrader, R. Gersonde, M. M. Drooger, and J. A. Broekman, pp. 129–176., 1978.

1096 Shevenell, A. E., Ingalls, A. E., Domack, E. W. and Kelly, C.: Holocene Southern Ocean surface temperature
1097 variability west of the Antarctic Peninsula, *Nature*, 470(7333), 250–254, doi:10.1038/nature09751, 2011.

1098 Siani, G., Michel, E., De Pol-Holz, R., DeVries, T., Lamy, F., Carel, M., Isguder, G., Dewilde, F. and Laurantou,
1099 A.: Carbon isotope records reveal precise timing of enhanced Southern Ocean upwelling during the last
1100 deglaciation, *Nature Communications*, 4(1), 2758, doi:10.1038/ncomms3758, 2013.

1101 Simpson, G. L. and Oksanen, J.: *Analogue: Analogue Matching and Modern Analogue Technique Transfer*
1102 *Function Models*. R Package Version 0.8-2, 2012.

1103 Sjunneskog, C. and Taylor, F.: Postglacial marine diatom record of the Palmer Deep, Antarctic Peninsula (ODP
1104 Leg 178, Site 1098) 1. Total diatom abundance, *Paleoceanography*, 17(3), PAL 4-1-PAL 4-8,
1105 doi:10.1029/2000PA000563, 2002.

1106 Stenni, B., Masson-Delmotte, V., Johnsen, S., Jouzel, J., Longinelli, A., Monnin, E., Röthlisberger, R. and

1107 Selmo, E.: An Oceanic Cold Reversal During the Last Deglaciation, *Science*, 293(5537), 2074–2077,
1108 doi:10.1126/science.1059702, 2001.

1109 Stenni, B., Buiron, D., Frezzotti, M., Albani, S., Barbante, C., Bard, E., Barnola, J. M., Baroni, M., Baumgartner,
1110 M., Bonazza, M., Capron, E., Castellano, E., Chappellaz, J., Delmonte, B., Falourd, S., Genoni, L., Iacumin, P.,
1111 Jouzel, J., Kipfstuhl, S., Landais, A., Lemieux-Dudon, B., Maggi, V., Masson-Delmotte, V., Mazzola, C.,
1112 Minster, B., Montagnat, M., Mulvaney, R., Narcisi, B., Oerter, H., Parrenin, F., Petit, J. R., Ritz, C., Scarchilli,
1113 C., Schilt, A., Schüpbach, S., Schwander, J., Selmo, E., Severi, M., Stocker, T. F. and Udisti, R.: Expression of
1114 the bipolar see-saw in Antarctic climate records during the last deglaciation, *Nature Geoscience*, 4(1), 46–49,
1115 doi:10.1038/ngeo1026, 2011.

1116 Stuiver, M., Reimer, P. J. and Reimer, R. W.: Calib 7.1, [online] Available from: <http://calib.org/> (Accessed 20
1117 November 2021), 2018.

1118 Thomas, Allen, Etourneau, King, Severi, Winton, Mueller, Crosta and Peck: Antarctic Sea Ice Proxies from
1119 Marine and Ice Core Archives Suitable for Reconstructing Sea Ice over the past 2000 Years, *Geosciences*, 9(12),
1120 506, doi:10.3390/geosciences9120506, 2019.

1121 Timmermann, A., Okumura, Y., An, S.-I., Clement, A., Dong, B., Guilyardi, E., Hu, A., Jungclaus, J. H.,
1122 Renold, M., Stocker, T. F., Stouffer, R. J., Sutton, R., Xie, S.-P. and Yin, J.: The Influence of a Weakening of the
1123 Atlantic Meridional Overturning Circulation on ENSO, *Journal of Climate*, 20(19), 4899–4919,
1124 doi:10.1175/JCLI4283.1, 2007.

1125 Totten, R. L., Fonseca, A. N. R., Wellner, J. S., Munoz, Y. P., Anderson, J. B., Tobin, T. S. and Lehrmann, A.
1126 A.: Oceanographic and climatic influences on Trooz Glacier, Antarctica during the Holocene, *Quaternary*
1127 *Science Reviews*, 276, 107279, doi:10.1016/j.quascirev.2021.107279, 2022.

1128 Turner, J., Orr, A., Gudmundsson, G. H., Jenkins, A., Bingham, R. G., Hillenbrand, C.-D. and Bracegirdle, T. J.:
1129 Atmosphere-ocean-ice interactions in the Amundsen Sea Embayment, West Antarctica, *Reviews of Geophysics*,
1130 55(1), 235–276, doi:10.1002/2016RG000532, 2017.

1131 Vancoppenolle, M., Meiners, K. M., Michel, C., Bopp, L., Brabant, F., Carnat, G., Delille, B., Lannuzel, D.,
1132 Madec, G., Moreau, S., Tison, J. L. and van der Merwe, P.: Role of sea ice in global biogeochemical cycles:
1133 Emerging views and challenges, *Quaternary Science Reviews*, 79, 207–230,
1134 doi:10.1016/j.quascirev.2013.04.011, 2013.

1135 Vaughan, D. G., Marshall, G. J., Connolley, W. M., Parkinson, C., Mulvaney, R., Hodgson, D. A., King, J. C.,
1136 Pudsey, C. J. and Turner, J.: Recent Rapid Regional Climate Warming on the Antarctic Peninsula, *Climatic*
1137 *Change*, 60(3), 243–274, doi:10.1023/A:1026021217991, 2003.

1138 Vernet, M., Martinson, D., Iannuzzi, R., Stammerjohn, S., Kozłowski, W., Sines, K., Smith, R. and Garibotti, I.:
1139 Primary production within the sea-ice zone west of the Antarctic Peninsula: I—Sea ice, summer mixed layer,
1140 and irradiance, *Deep Sea Research Part II: Topical Studies in Oceanography*, 55(18–19), 2068–2085,
1141 doi:10.1016/j.dsr2.2008.05.021, 2008.

1142 Vorrath, M.-E., Müller, J., Esper, O., Mollenhauer, G., Haas, C., Schefuß, E. and Fahl, K.: Highly branched
1143 isoprenoids for Southern Ocean sea ice reconstructions: a pilot study from the Western Antarctic Peninsula,
1144 *Biogeosciences*, 16(15), 2961–2981, doi:10.5194/bg-16-2961-2019, 2019.

1145 Vorrath, M.-E., Müller, J., Rebolledo, L., Cárdenas, P., Shi, X., Esper, O., Opel, T., Geibert, W., Muñoz, P.,
1146 Haas, C., Kuhn, G., Lange, C. B., Lohmann, G. and Mollenhauer, G.: Sea ice dynamics in the Bransfield Strait,
1147 Antarctic Peninsula, during the past 240 years: a multi-proxy intercomparison study, *Climate of the Past*, 16(6),
1148 2459–2483, doi:10.5194/cp-16-2459-2020, 2020.

1149 WAIS Divide Project Members: Onset of deglacial warming in West Antarctica driven by local orbital forcing,
1150 *Nature*, 500(7463), 440–444, doi:10.1038/nature12376, 2013.

1151 WAIS Divide Project Members: Precise inter-polar phasing of abrupt climate change during the last ice age,
1152 *Nature*, 520(7549), 661–665, doi:10.1038/nature14401, 2015.

1153 Warnock, J. P. and Scherer, R. P.: A revised method for determining the absolute abundance of diatoms, *Journal*
1154 *of Paleolimnology*, 53(1), 157–163, doi:10.1007/s10933-014-9808-0, 2015.

1155 Wefer, G., Fischer, G., Fütterer, D. and Gersonde, R.: Seasonal particle flux in the Bransfield Strait, Antarctica,
1156 *Deep Sea Research Part A. Oceanographic Research Papers*, 35(6), 891–898, doi:10.1016/0198-0149(88)90066-
1157 0, 1988.

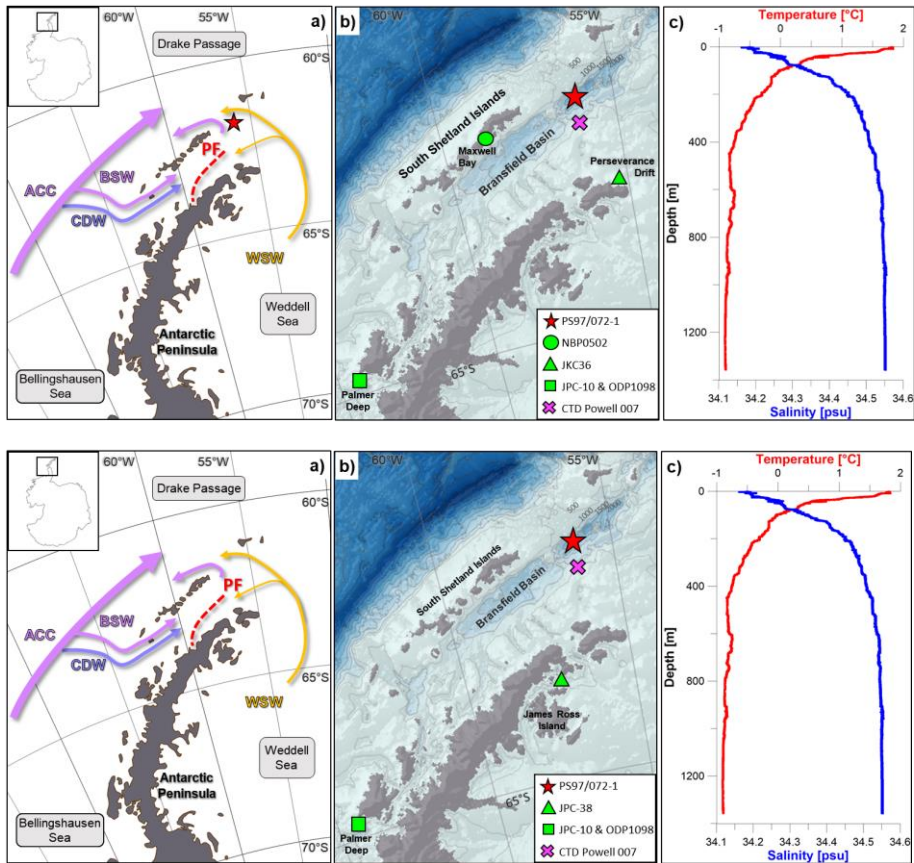
1158 Wu, S., Kuhn, G., Diekmann, B., Lembke-Jene, L., Tiedemann, R., Zheng, X., Ehrhardt, S., Arz, H. W. and
1159 Lamy, F.: Surface sediment characteristics related to provenance and ocean circulation in the Drake Passage
1160 sector of the Southern Ocean, *Deep Sea Research Part I: Oceanographic Research Papers*, 154, 103135,
1161 doi:10.1016/j.dsr.2019.103135, 2019.

1162 Zielinski, U. and Gersonde, R.: Diatom distribution in Southern Ocean surface sediments (Atlantic sector):
1163 Implications for paleoenvironmental reconstructions, *Palaeogeography, Palaeoclimatology, Palaeoecology*,
1164 129(3–4), 213–250, doi:10.1016/S0031-0182(96)00130-7, 1997.

1165 Zwally, H. J., Comiso, J. C., Parkinson, C. L., Cavalieri, D. J. and Gloersen, P.: Variability of Antarctic sea ice
1166 1979–1998, *Journal of Geophysical Research*, 107(C5), 3041, doi:10.1029/2000JC000733, 2002.

1167

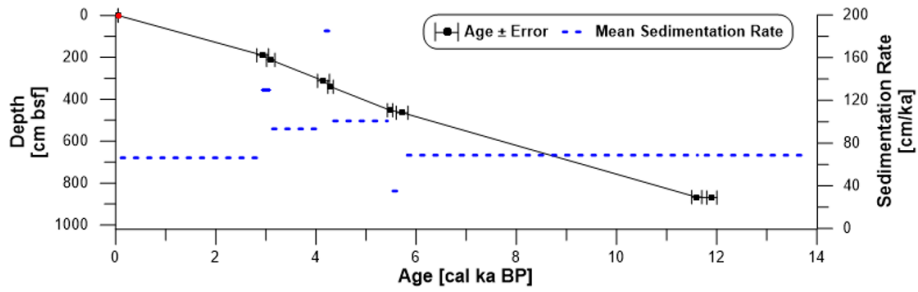
1168



1170

1171

1172 Figure 1: a) Overview map with modern oceanography in the study area (Hofmann et al., 1996; Sangrà et al., 2011). ACC =
 1173 Antarctic Circumpolar Current, BSW = Bellingshausen Sea Water, CDW = Circumpolar Deep Water, WSW = Weddell Sea
 1174 Water, and PF = Peninsula Front. b) Bathymetric features in the Bransfield Strait with the location of sediment core PS97/072-
 1175 1 (red star) and other sediment records discussed in the text (green), and the CTD station (purple cross) where c) the vertical
 1176 profile of ocean temperature and salinity (cruise POWELL2020, CTD 007 (62°09.075'S, 56°37.09'W) from 27.01.2020) shows
 1177 a clear stratification of the upper 100 m of the water column. It indicates that surface waters are dominated by the BSW, while
 1178 the basin is filled with WSW water. Maps were done with QGIS 3.0 (QGIS, 2018) and the bathymetry was taken from
 1179 GEBCO_14 from 2015.

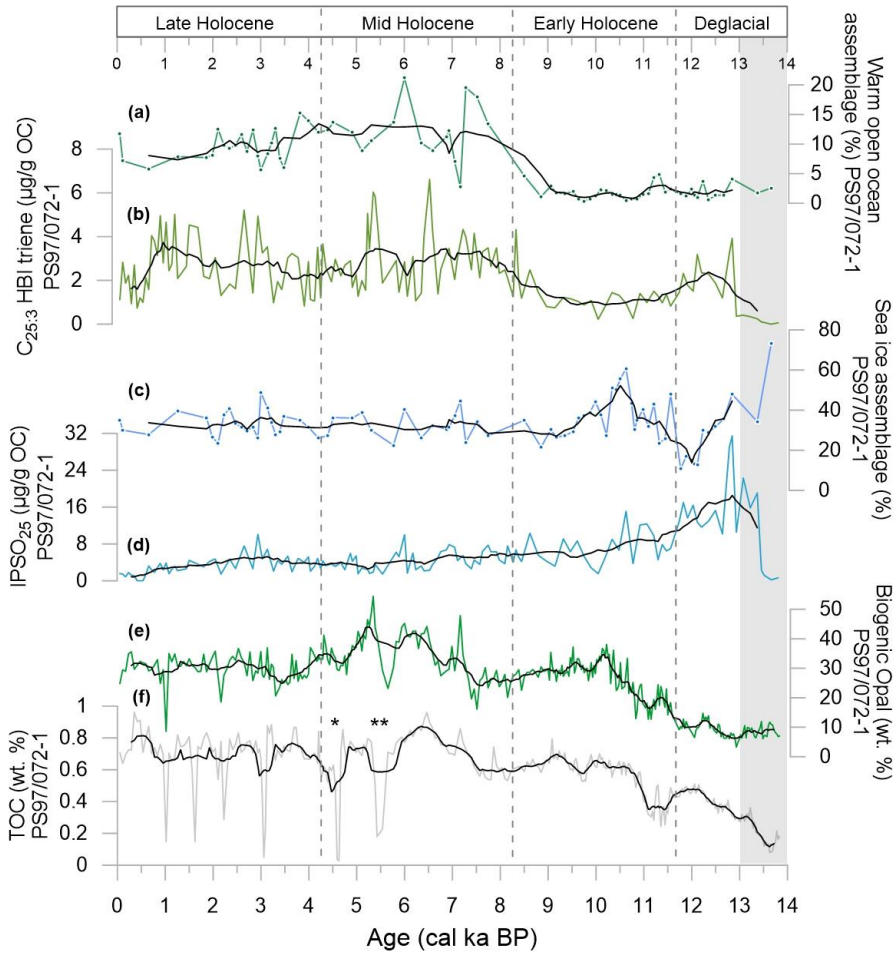


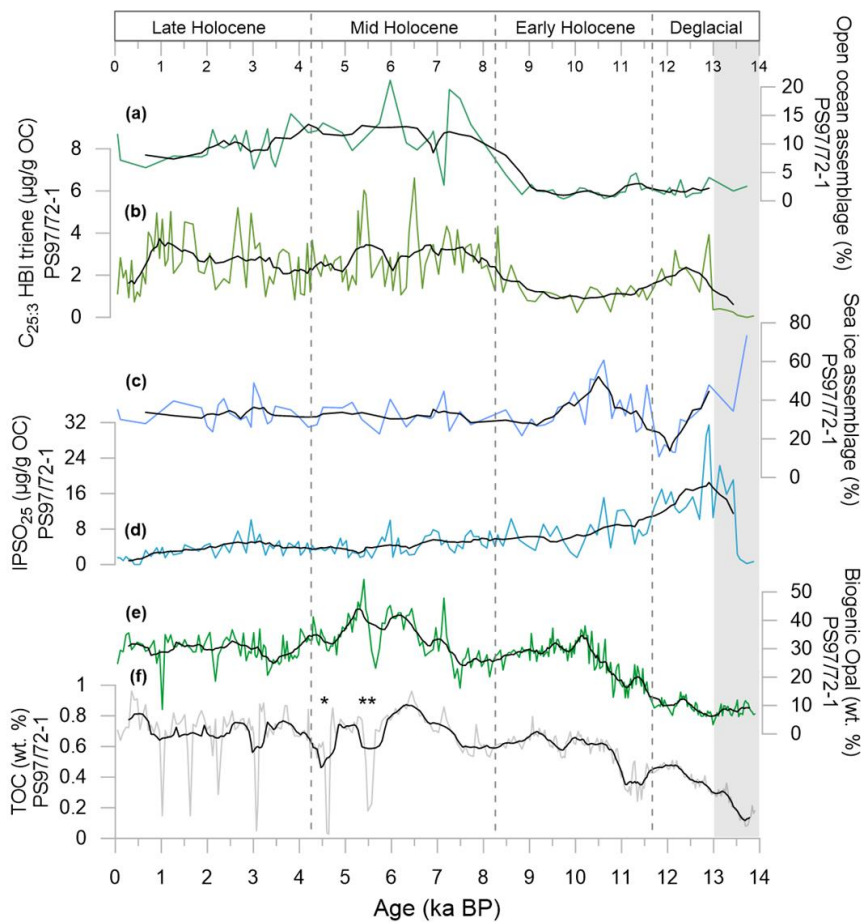
1180
1181

1182 Figure 2: Age-depth model for sediment core PS97/072-1 based on eight ^{14}C dated calcite samples (black) with
 1183 error bars and mean sedimentation rates (cm/ka, dashed blue line). The core top age (red) was estimated as 0.05
 1184 ka BP from matching with the ^{210}Pb -dated multicore PS97/072-2 (Vorrath et al., 2020; see supplement section 2).

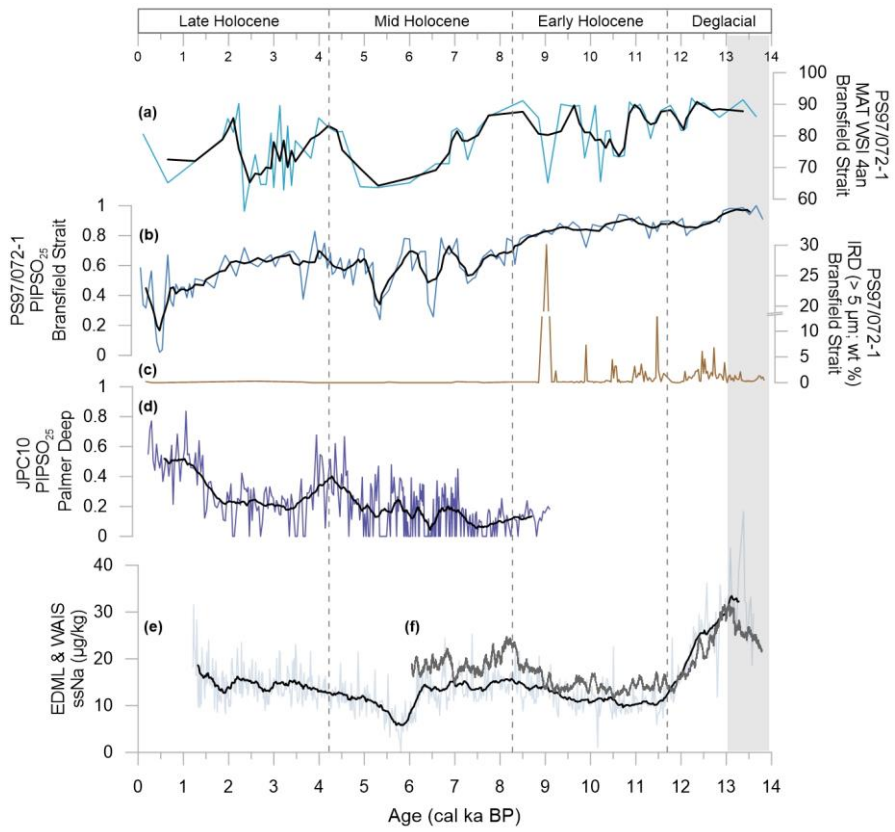
1185

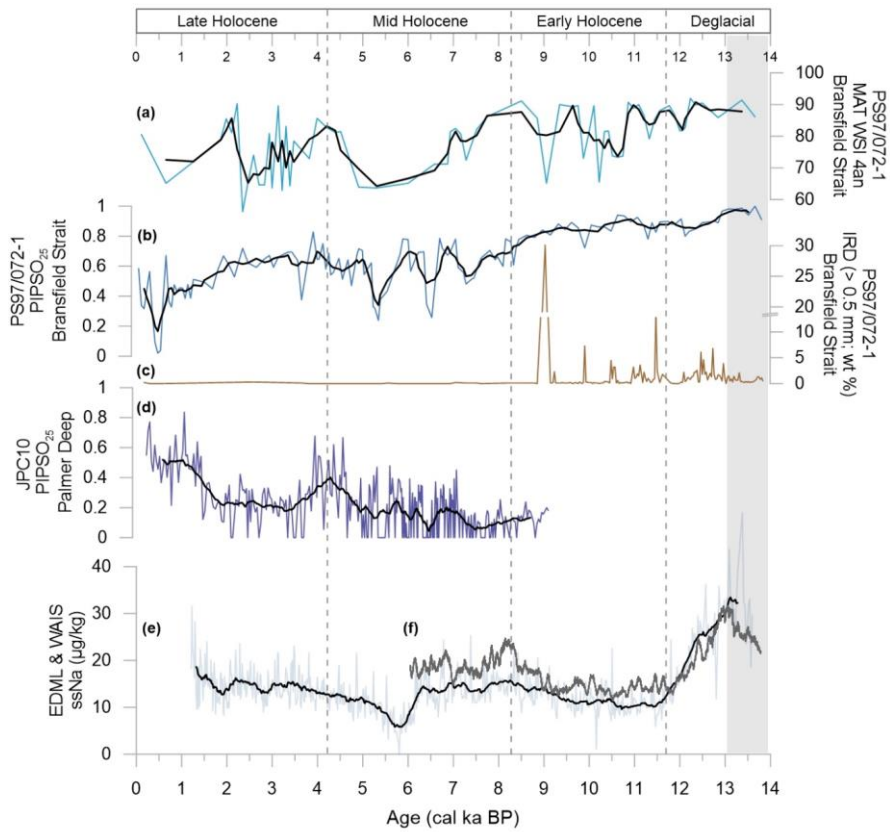
1186





1188
 1189 Figure 3: Overview of organic geochemical parameters and main diatom assemblages determined in sediment core
 1190 PS97/072-1 used to characterize the environmental setting over the past 14 ka BP. a) warm open ocean diatom
 1191 assemblage, b) C_{25:3} HBI triene, c) sea ice diatom assemblage, d) IP SO₂₅, e) biogenic opal and f) TOC contents.
 1192 Asterisks in f) mark layers of volcanic ash, where ** can be linked to a tephra layer in a sediment core from the
 1193 Bransfield Strait at 5.5 ka BP (Heroy et al., 2008). Black lines display running averages. Grey shaded interval
 1194 refers to the Antarctic Cold Reversal.





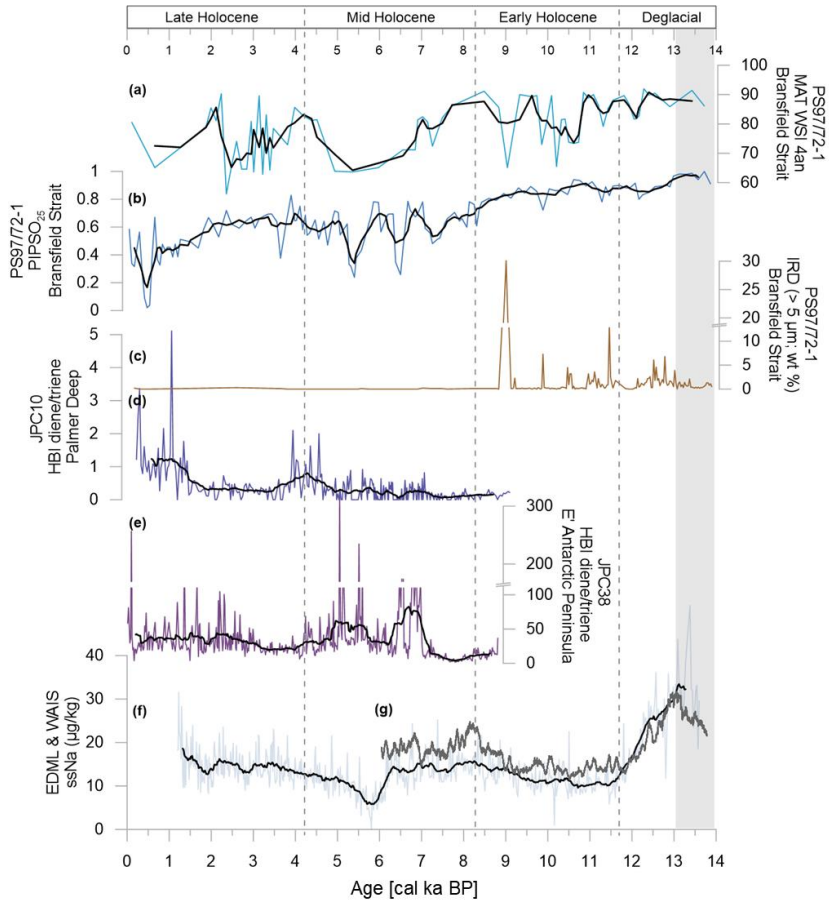
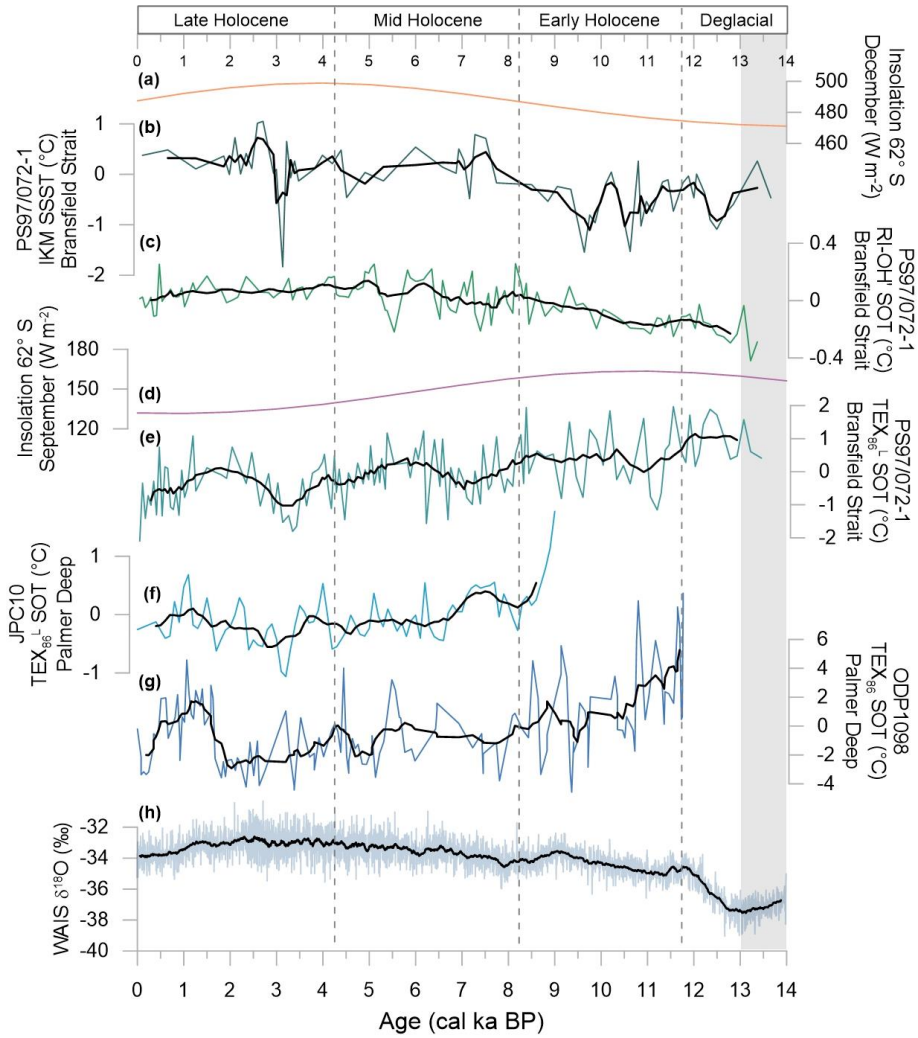


Figure 4: Sea ice related proxies in sediment core PS97/072-1 with a) the diatom based WSI, b) the [sea-ice-sea-ice](#) index PIPSO₂₅, and c) ice rafted debris (IRD). For comparison: [PIPSO₂₅ values](#) ~~the HBI diene/triene ratio~~ of sediment core d) JPC10 from the Palmer Deep station (Etourneau et al., 2013) and e) [JPC38 at the East Antarctic Peninsula](#) (Barbara et al., 2016). ~~ssNa records of~~ [the EDML ice core](#) (Fischer et al., 2007) and [the WAIS ice core](#) (WAIS Divide Project Members, 2015). [Black lines display running averages](#). Grey shaded interval refers to the [Antarctic Cold Reversal](#).



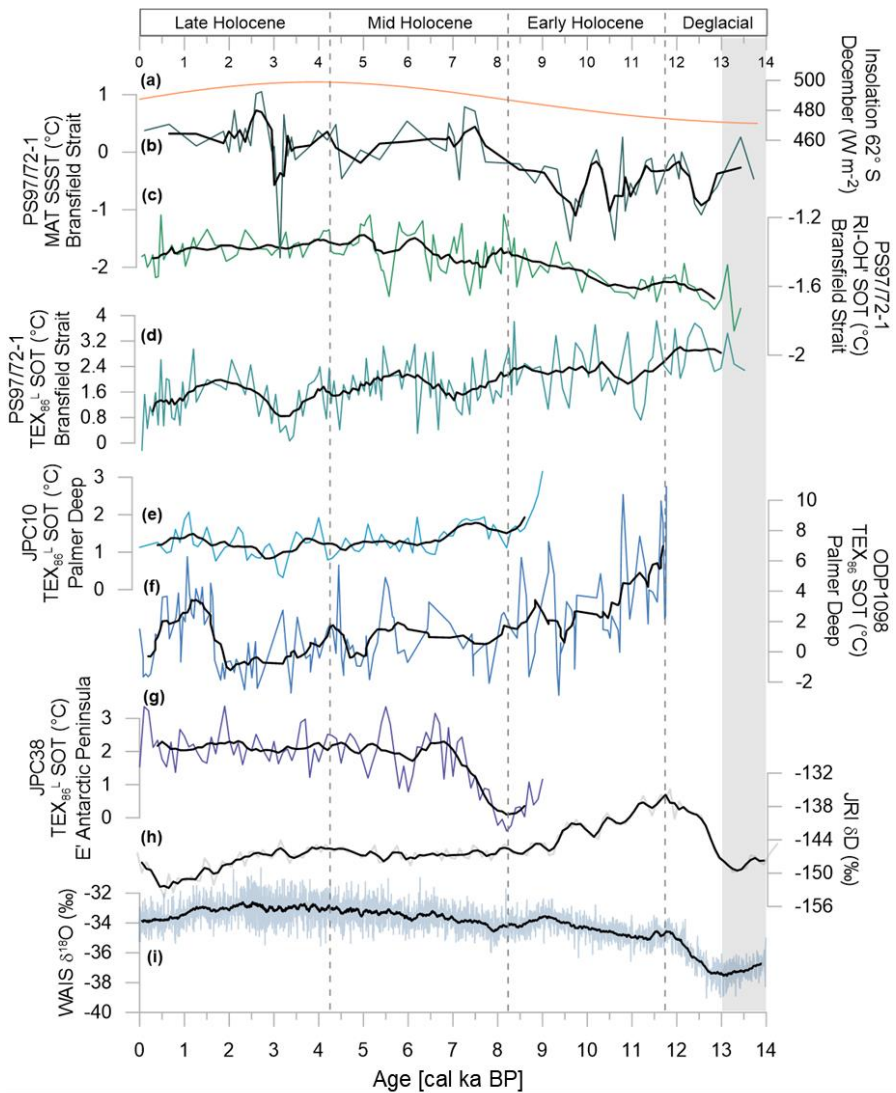


Figure 5: A comparison of a) December insolation (Laskar et al., 2004), b) diatom-based SSTS, c) RI-OH⁺-derived SOT, d) September ~~Spring~~-insolation (Laskar et al., 2004), e) TEX₈₆^l-SOT of sediment core PS97/072-1, and temperature reconstructions f) TEX₈₆^l from JPC10, Palmer Deep (Etourneau et al., 2013), g) TEX₈₆^l from ODP1098, Palmer Deep (Shevenell et al., 2011), e) TEX₈₆^l from JPC38, East Antarctic Peninsula, and h) ice core stable isotope records of h) JRI (Mulvaney et al., 2012) and i) WAIS Divide (WAIS Divide Project Members, 2013). Ocean temperatures are displayed as anomalies with respect to the mean of the individual SOT and SSST

- Formatiert: Schriftart: Nicht Fett
- Formatiert: Schriftart: Nicht Fett
- Formatiert: Schriftart: Nicht Fett
- Formatiert: Schriftart: Nicht Fett
- Formatiert: Schriftart: Nicht Fett
- Formatiert: Schriftart: Nicht Fett
- Formatiert: Schriftart: Nicht Fett
- Formatiert: Schriftart: Nicht Fett
- Formatiert: Schriftart: Nicht Fett
- Formatiert: Schriftart: Nicht Fett
- Formatiert: Schriftart: Nicht Fett
- Formatiert: Schriftart: Nicht Fett
- Formatiert: Schriftart: Nicht Fett
- Formatiert: Schriftart: Nicht Fett
- Formatiert: Schriftart: Nicht Fett
- Formatiert: Schriftart: Nicht Fett
- Formatiert: Schriftart: Nicht Fett
- Formatiert: Schriftart: Nicht Fett
- Formatiert: Schriftart: Nicht Fett
- Formatiert: Schriftart: Nicht Fett
- Formatiert: Schriftart: Nicht Fett
- Formatiert: Schriftart: Nicht Fett
- Formatiert: Schriftart: Nicht Fett
- Formatiert: Schriftart: Nicht Fett
- Formatiert: Schriftart: Nicht Fett
- Formatiert: Schriftart: Nicht Fett
- Formatiert: Schriftart: Nicht Fett
- Formatiert: Schriftart: Nicht Fett
- Formatiert: Schriftart: Nicht Fett
- Formatiert: Schriftart: Nicht Fett
- Formatiert: Schriftart: Nicht Fett
- Formatiert: Schriftart: Nicht Fett
- Formatiert: Schriftart: Nicht Fett
- Formatiert: Schriftart: Nicht Fett
- Formatiert: Schriftart: Nicht Fett
- Formatiert: Schriftart: Nicht Fett
- Formatiert: Schriftart: Nicht Fett
- Formatiert: Schriftart: Nicht Fett
- Formatiert: Schriftart: Nicht Fett
- Formatiert: Schriftart: Nicht Fett

1216 values of the entire record. Black lines display running averages. Grey shaded area refers to the Antarctic Cold
1217 Reversal.4
1218

Formatiert: Schriftart: Nicht Fett

Formatiert: Schriftart: Nicht Fett